4-20-2020

Investigation of Water Vapor Transport in Membrane Mass Exchangers for HVAC Applications

Nathan DeMario
ncd4192@rit.edu

RIT

Investigation of Water Vapor Transport in Membrane Mass Exchangers for HVAC Applications

by

Nathan DeMario

A Thesis Submitted in Partial Fulfillment of the Requirements for the Degree of Master of Science in Engineering

Department of Mechanical Engineering

Kate Gleason College of Engineering

Rochester Institute of Technology

Rochester, NY

April 20, 2020

Committee Approval:

_____

Dr. Ali Ogut, Professor Date

Thesis Advisor, Department of Mechanical Engineering

_____

Dr. Jason Kolodziej, Associate Professor Date

Committee Member, Department of Mechanical Engineering

_____

Dr. Robert Stevens, Associate Professor Date

Committee Member, Department of Mechanical Engineering

_____

Dr. Michael Schrlau, Associate Professor Date

Committee Member, Department of Mechanical Engineering

Abstract

Vapor compression systems have dominated the HVAC area for close to 100 years. These systems require significant amounts of energy to complete the compression cycle and the refrigerants used are known contributors to global warming. As a result, new innovations are being sought and a membrane-based system, the subject of this thesis, is one such technology. Water selective membrane materials offer a promising alternative to vapor compression for dehumidification of building air. For HVAC systems, process air pressure drop constrains flow path design in a membrane-based approach. The transport resistance for water vapor from air flow channels is experimentally investigated for a plate-type membrane mass exchanger design. Convective and diffusive resistances are measured for polymer membranes with varying flow channel dimensions. A series of experiments and analyses is developed to separate diffusive and convective transport resistance to water vapor removal from supply air. Results are compared with empirical Sherwood number correlations to enable improved mass exchanger design. The validated mass transfer correlations were used to develop a mass transfer model and later implemented for the simulation of a 3 rTon (1 rTon = 3.516kW) membrane heat pump dedicated outdoor air systems. From the various analyses, maintaining process air pressure drop at less than 50 Pa while at a typical HVAC face velocity results in a convective resistance that is 6 times greater than the diffusive resistance to water vapor through an ionic membrane. Furthermore, the trade-off between required membrane area, system size, pressure-drop and effective latent cooling is explored. Simulation results show that when conforming mass exchanger designs to meet ASHRAE standards, a system electrical COP of 7.5 or greater can be achieved.

Acknowledgements

First and foremost, I would like to thank my thesis advisor Dr. Ali Ogut. His time and guidance were invaluable throughout my time at RIT. I would also like to thank my thesis committee, Dr. Kolodziej, Dr. Stevens, and Dr. Schrlau for their support of my work.

My interest in research, and more specifically research in membrane cooling systems was sparked during my time at Alfred State College with Dr. Jon Owejan. Dr. Owejan taught me the importance of developing well designed experiments. Additionally, he has pushed me to strive for perfection and take pride in the work I am completing. Without his support, I would not be where I am today. I must thank Dr. Owejan for introducing me to entrepreneurship. Together we were able to start a company and have had the opportunity to work with many great organizations such as NYSERDA, NextCorps, and Venture Creations to assist in the development of advanced HVAC technologies. Additionally, I have been able to work with a great team including Brian Mothon, Daniel Crosby, and Brendon DeClerck who have all provided great humor and support.

To my fiancé, Kelly Stieve, thank you for all your support. You push me every day to be the best I can and to work my hardest. Lastly, I would like to thank my sister and my parents for their support. My parents have been a solid foundation for my education. My mother was my high school AP Chemistry, Regents Chemistry, and Regents Physics teacher who taught me the foundation of engineering laws and principles. My father provided me with my work ethic and my ability to build. Their continued support for me to pursue my goals has never wavered.

Table of Contents

List of Figures

List of Tables

Nomenclature

$AC = Air\ Conditioning$

$ASHRAE$

$= American\ Standards\ for\ Heating, Refridgeration, and\ Air\ Conditioning\ Engineers$

$COP = Coefficient\ of\ Performance$

$DOAS = Dedicated\ Outdoor\ Air\ System$

$EER = Energy\ Efficiency\ Ratio$

$GWP = Global\ warming\ potential$

$HVAC = heating, ventilation\ and\ air\ conditioning$

$LD = Liquid\ Desiccant$

$ME = Mass\ Exchanger$

$MHP = Membrane\ Heat\ Pump$

$P = Pressure$

$PFSA = Perfluoro\ Sulfinated\ Acid$

$QUAD = 1.055 \times 10^{18}\ Joules$

$RH = Relative\ Humidity$

$rTon = 3.516\ kW\ of\ Cooling$

$SEER = Seasonal\ Energy\ Efficiency\ Ratio$

$T = Temperature$

$VI = Virtual\ Interface$

1. Introduction

Air conditioning (AC) accounts for a significant portion of the energy delivered to residential and non-residential buildings. Over 20% of energy consumed in buildings is used for cooling [1]. In tropical climates where most of the world's population lives, the majority of this energy is used for dehumidification with a latent to sensible ratio typically greater than 3:1 [2]. The most common systems currently deployed throughout the globe are vapor compression heat pumps that evaporate and condense refrigerants to remove heat and humidity from supply air. The refrigerants used in these systems are known contributors to global warming. The most common refrigerants, R-134A, R407C and R-404A have 2000 times more global warming potential than carbon dioxide [3]. Vapor compression systems also use electricity to power the compressor. For this reason, electricity grids at macro and micro scales are ultimately sized for the highest annual sensible and latent cooling load in many regions. As a result, the potential environmental and infrastructural impact of alternative cooling technologies that do not require refrigerants or high electrical power are substantial.

The most common way of removing heat and humidity from air is through contact with an extended surface that is held at a low dew point by either directly or indirectly evaporating a refrigerant. The energy required for this process is first constrained by the heat of vaporization to condense water. Further, the process overcools air and requires postprocess heat input in many applications. Humidity control with water transfer membranes can eliminate these energy requirements associated with condensing systems. Numerous membrane materials have been shown effective for water selectivity and high water transfer flux [4–8].

Researchers have studied numerous system mechanizations aimed at utilizing membranes for AC applications [9,10]. All of these concepts are designed to diffuse water vapor through the

membrane by creating a concentration gradient. Vacuum systems reduce the total pressure on the dry side of the membrane and exhaust water vapor from the pump outlet [11,12]. Membrane heat pumps are similar to vacuum-based approaches except the pressure ratio is reduced by using a second membrane at the pump outlet [13,14]. Membrane separators are also being used with a variety of liquid desiccants [15]. Isolating the desiccant solution greatly reduces carry over of salt and improves performance by enabling a higher free surface area of the solution.

Regardless of how a membrane AC system is designed, the mass transfer (or separation) of water vapor from the supply air is a critical challenge. Maximizing mass transfer while avoiding the energy penalty of high pressure drop results in carefully designed flow paths for supply air through the mass exchanger. ASHRAE Standard 62 sets the standards for some HVAC components for use in commercial building ventilation systems. For Finned-Tube Coils, the pressure drop through the coil cannot exceed 187 Pa (0.75 in. w.c.) when combined and face velocity cannot exceed 2.54 m/s [16]. For residential systems, the combined pressure drop that a fan must overcome is 250 Pa (1 in. w.c.) [17]. These constraints of pressure drop, and face velocity are used when determining the channel dimensions and channel length for a membrane system, however, to date there is limited published materials on the effects of channel dimensions on membrane heat pump performance.

In this study, the membrane water vapor transfer is measured and used to evaluate the effects of channel resistance on mass transfer performance. A low-pressure differential evaluation consisting of two air streams, one humid (wet) and one dry, is completed with varying feed rates. A second evaluation is used to evaluate the performance of a proposed section of a membrane heat pump, the latent mass exchanger [13,14]. A single air stream is delivered to a mass exchanger with a vacuum held on the opposing side of the membrane. This sequence of testing allows for

the channel's diffusion resistance to be modeled separately from the membrane's diffusion resistance. Of the many studies that evaluate membrane heat pump performance [11,12,14,18,19], there have been few reports on the rate of mass transfer as convective resistance in the channel of a mass exchanger is varied. The observed results were used to validate a down the channel mass transfer model and later applied to a system model of a 3 rTon Membrane Heat Pump (MHP) Dedicated Outdoor Air System (DOAS) where the Coefficient of Performance (COP) of multiple mass exchangers were compared under the same working conditions. As a result, the tradeoff between the decrease of in-channel convective resistance to the energy penalty of pressure drop is discussed.

2. Literature Review

Current literature has limited studies that focus on optimizing MHP performance to the current design constraints of an HVAC system. Current HVAC components rely on minimal pressure drop through each component while maximizing mixing to overcome convective resistance. The performance of an MHP is highly dependent upon the membrane material, channel geometry, pressure drop, and pump(s) efficiency. The following sections will provide substantial background on the current state of the technology and on the phenomenon that occur in an MHP system.

2.1 Overview of HVAC Energy Consumption and Current Refrigerants

Of the 5645 quadrillion joules of energy used relating to commercial HVAC, 29% of this energy is consumed in conditioning the outdoor air to match desired indoor air conditions (ventilation) and another 28% of this energy is used to maintain the desired indoor conditions in the form of space cooling (Figure 1). This totals to 3197 quadrillion joules annually and based on analyses by the United States Department of Energy, nearly all of this cooling power is delivered with electricity [19]. The impinging energy load strains the grid often causing failure. The best method to improve grid reliability is to reduce energy consumption. The current method of over cooling to condense water followed by reheat has become more efficient through the use of variable speed compressors [20]. However, independent control of latent and sensible cooling eliminates the need for post process heat input while avoiding the high energy cost of phase change.

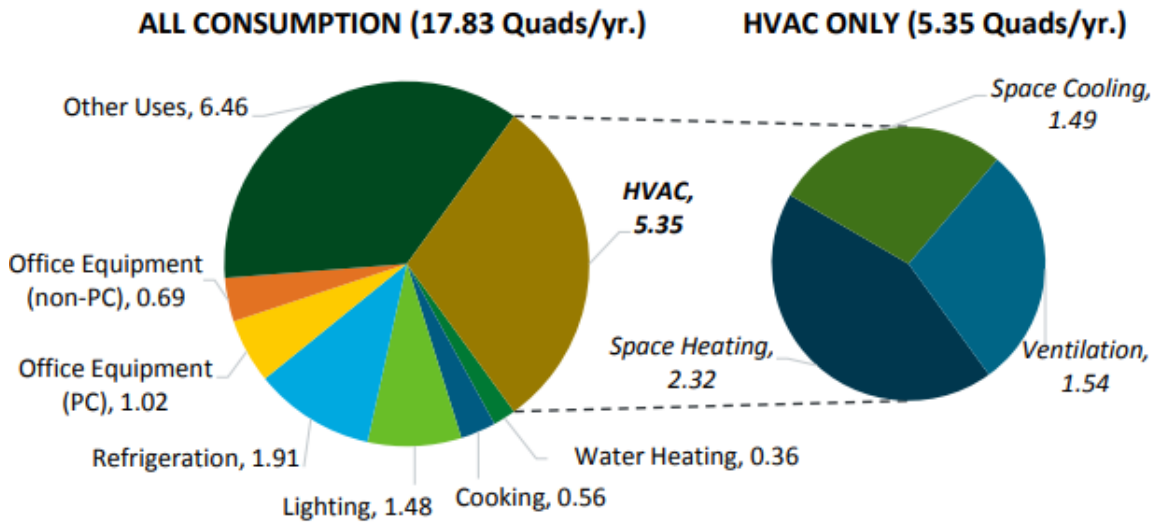

Figure 1: Commercial primary energy consumption by end use, Quads/yr. [19]

The increase in concern from global warming has persuaded governments and regulatory bodies to ban the use of refrigerants such as R12 and R22 known for their excellent vapor compression properties. While the current class of refrigerants such as R134A, R410A and R407C yield sufficient thermal properties, their global warming potential (GWP) are all greater than 1000 [21]. As a result, there has been much interest in the development of new technology which would not require the use of refrigerants while improving the efficiency of HVAC systems.

2.2 Membrane Cooling Systems

Newly introduced technologies for reducing energy consumption relating to HVAC have showed promising futures. Liquid Desiccant systems and Membrane Heat Pumps have been reviewed as "most promising" and "very promising" alternatives to vapor compression by the Department of Energy in 2014 [14]. The following sub-sections will provide more detail on each system and the current technology outlook.

2.2.1 Liquid Desiccants

Liquid desiccant systems use liquid salts such as lithium chloride or calcium chloride to absorb water vapor from the supply air [19]. The liquid desiccant is circulated from a conditioner

to a regenerator. The transfer of water vapor out of the supply air is driven by vapor pressure gradients. The break lines in Figure 2 represent the presence of a porous, hydrophobic membrane. Supply air is conditioned as it moves through the air flow channels and is then sent to the building. The diluted liquid desiccant is then heated in preparation of regeneration as it moves to a regenerator. The regenerator supplies process, ambient air on the opposing side of a porous, hydrophobic membrane from the diluted liquid desiccant. The water vapor then moves from the liquid desiccant solution into the process ambient air. [9]

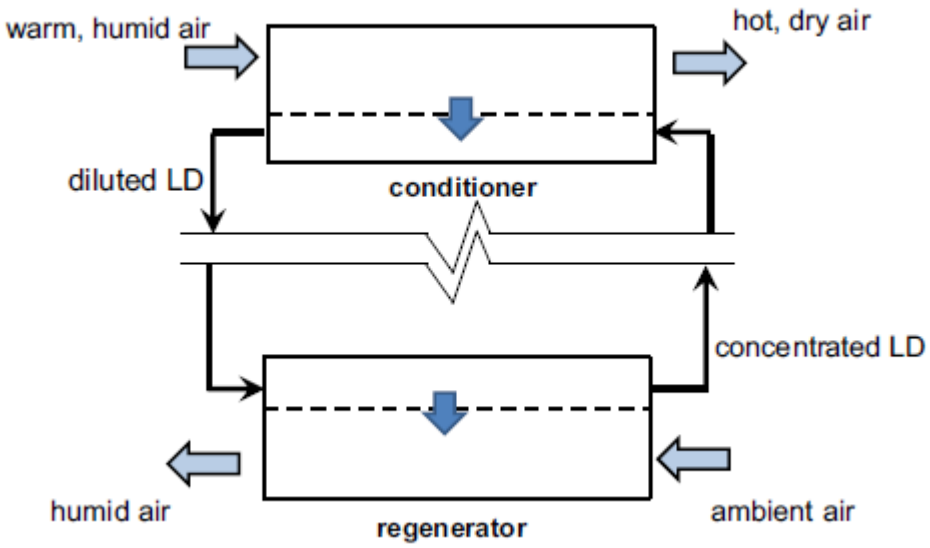

Figure 2: Schematic of liquid desiccant dehumidification [9]

The energy saving of a liquid desiccant system is provided by the removal of water vapor without phase change and from the limited amount of cooling required as the regenerated liquid desiccant returns to the conditioner. If the heat required for the regeneration in liquid desiccant system is provided by an existing heat source, a significant energy savings can be produced for building owners. The current barriers to market for liquid desiccant systems is the lack of design concepts suitable for large scale manufacturing, reliability, and maintenance. [14]

2.2.2 Membrane Heat Pump

The membrane heat pump is comprised of a dehumidification mass exchanger, a compressor, and an expirator mass exchanger. The dotted lines in Figure 3 represent a highly selective membrane designed for water vapor transfer. Water vapor movement is provided using pressure gradients in each mass exchanger. As air enters the dehumidification mass exchanger, water vapor that is present in the supply air moves to the low-pressure plenum through the membrane. This plenum is maintained at approximately 1.25 kPa absolute. The water vapor is then pushed to the expirator through a compressor at a compression ratio of 2.3. The vapor pressure in the expirator low pressure plenum is approximately 3.5kPa. The water vapor in the plenum is removed by passing process air from the outdoors to accept the water vapor through the membrane. [9]

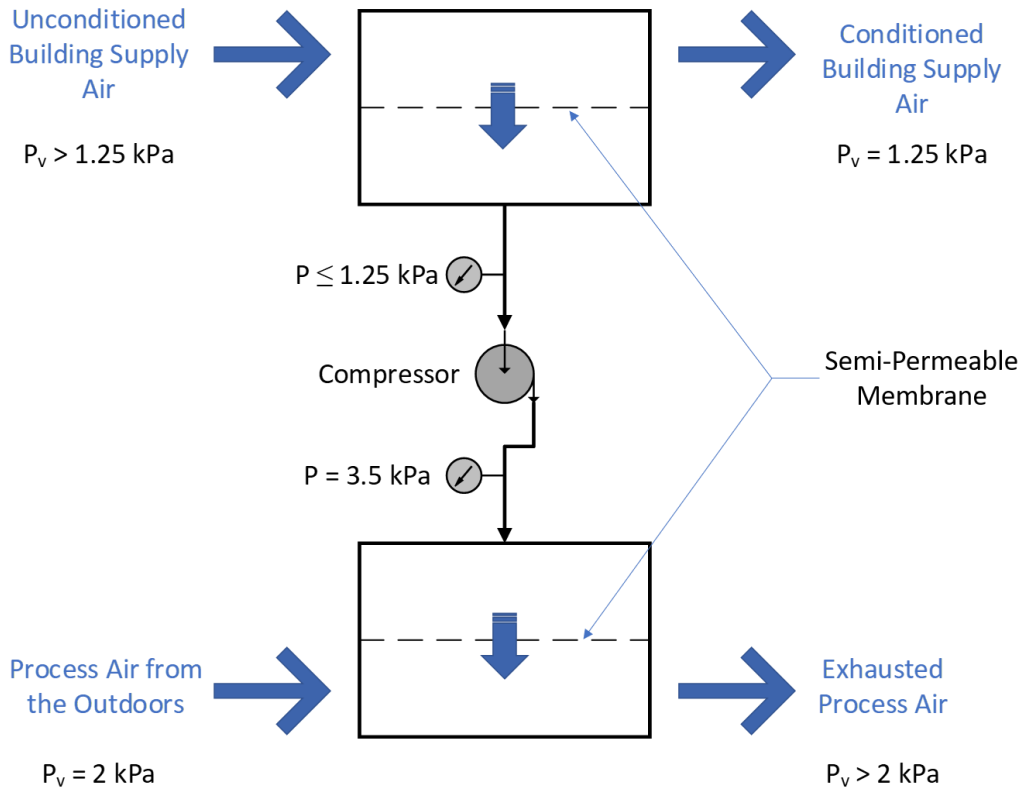

Figure 3: A membrane heat pump concept presented by DIAS (Adapted from [22]*)*

The current state of membrane heat pumps has provided much interest as a 7.5-ton capacity prototype at Oakridge National Lab has produced results that relate to a 50% energy savings over current vapor compression technology. Current barriers to entry for the MHP include complex membrane assemblies, durability concerns, and expensive compressors [19]. A further review of the membrane heat pump will be presented through the upcoming sections.

2.3 MHP History

Researchers have studied numerous system mechanizations aimed at utilizing membranes for AC applications [9,11,12,18,23]. All these concepts are designed to diffuse water vapor through the membrane by creating a concentration gradient. Vacuum systems reduce the total pressure on the dry side of the membrane and exhaust water vapor from the pump outlet.

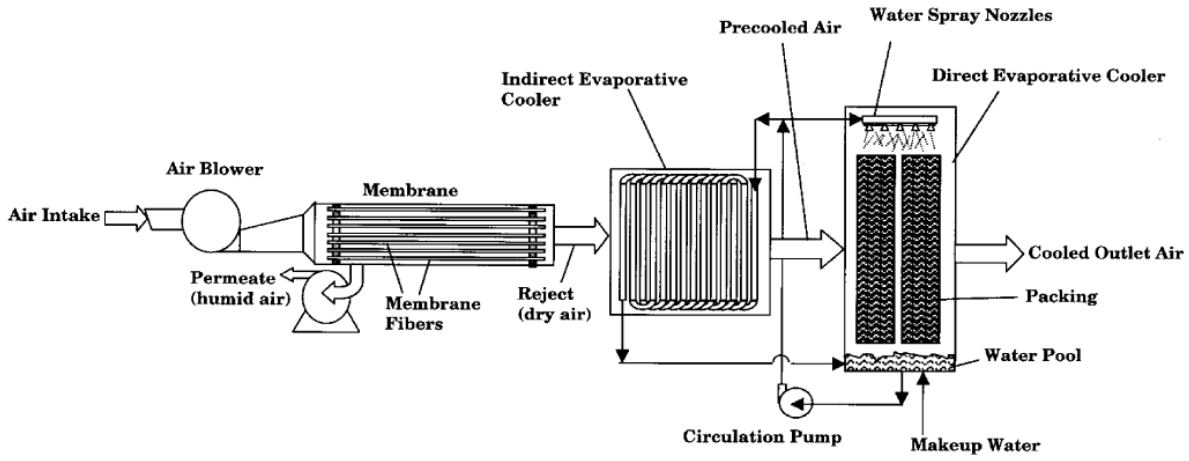

Figure 4: Membrane air drying combined with indirect/direct evaporative cooling [12].

The idea of a membrane dehumidifier was first presented by NASA where it was necessary to recover the moisture from the air [24]. Since the concept was first presented, the cost of the membranes has significantly reduced making a membrane cooling system more feasible. Early systems focused on using only a single mass exchanger for dehumificiation and a vacuum pump in conjunction with an indirect or direct evaporative cooler as seen in Figure 4 [12].

Another membrane-based dehumidification device was comprised of a single mass exchanger for dehumidification and a vacuum pump where the low-pressure side of the mass exchanger was fed through a gas sweeping process. After supply air passed through the mass exchanger the air was passed through a flow splitter. The flow splitter allows for air to be supplied to the room or to an expansion valve that leads to the low-pressure side of the mass exchanger. A system diagram can be seen in Figure 5 [11]. The use of a sweeping gas requires an increase in the pump power resulting in a tradeoff between humidity removal and dehumidification efficiency making it less feasible [18].

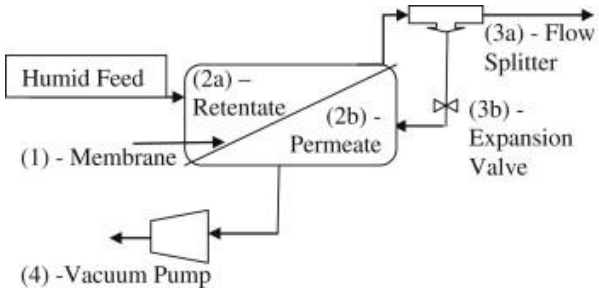

Figure 5: Vacuum Sweep Dehumidification System [11]

The previous membrane systems rely on a pump with a high-pressure ratio to maintain the low-pressure environment. Membrane heat pumps are similar but they reduce the pressure ratio with a membrane at the pump outlet [11,18]. In a project funded by the Department of Energy, Dais Analytic and others developed a membrane based latent and sensible cooling system. This system can be seen in Figure 6. Outdoor air in this system enters first into a membrane dehumidifier. The membrane dehumidifier is maintained at a pressure to promote water vapor transfer from the hot, wet outdoor air to the low-pressure side of the system. The dehumidified air is then sent to an air-water heat exchanger which cools the air to the sensible setpoint. The air-water heat exchanger receives cold water from a membrane evaporator unit. The membrane evaporator unit supplies liquid water to a membrane that is communicating with the low-pressure

environment. The water vapor captured in the dehumidifier and evaporator is moved through a vacuum pump towards an external membrane unit to be rejected to ambient. The vacuum pump raises the pressure of the water vapor that is passing through the pump, moving towards the outdoor membrane unit. Within the outdoor membrane unit, water vapor exits the low-pressure environment of the heat pump and is transferred into ambient air. The vacuum pump is crucial to the performance of the outdoor membrane unit as it raises the vapor pressure of the contained vapor environment above the vapor pressure of the air passing through. As a result of the lower compression ratio, system simulations have yielded an EER of 16 – 20. [18]

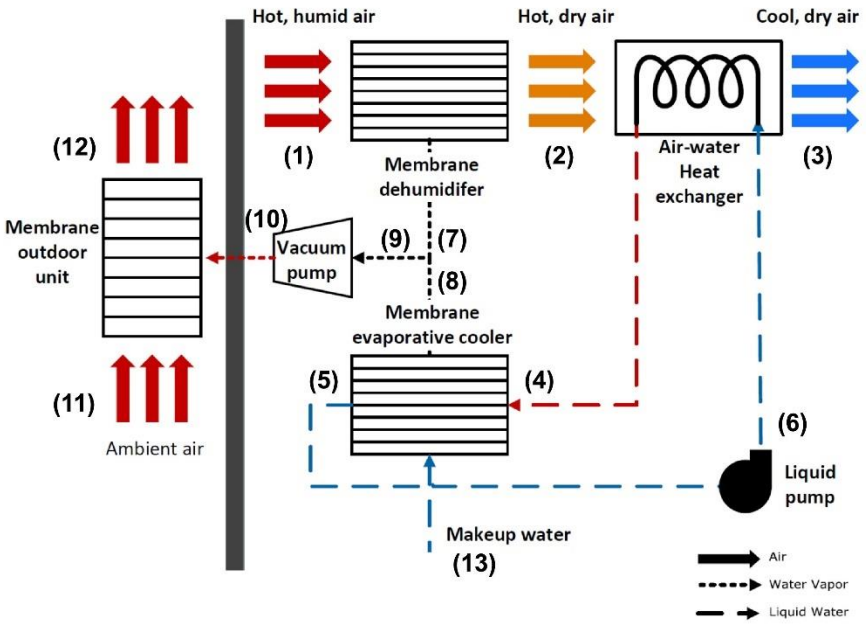

Figure 6: Proposed design by DIAS Analytic [18]

Another configuration of a membrane heat pump can be seen in Figure 7. Like the system designed by Dias Analytics, there are three membrane modules that function as the dehumidifier, chiller/evaporator and an expiration system. The key difference is the location of the vacuum pump and the air supplied to the expiration system. The vacuum pump is used to roughen the system to the proper operating pressure of approximately 1.275 kPa. Once at operating pressure,

the vacuum pump is shut off and isolated from the low-pressure environment. To maintain the low-pressure environment, hot and dry air is supplied to the expirator. The humidity ratio of the expiration supply air should be less than $8.0 g_{water\ vapor}/kg_{dry\ air}$ to sufficiently promote water vapor removal from the low-pressure environment. As water vapor enters to the low pressure environment it is moved to the expirator where it transfers out of the low pressure environment and into the hot, dry process air passing through the expirator. [13]

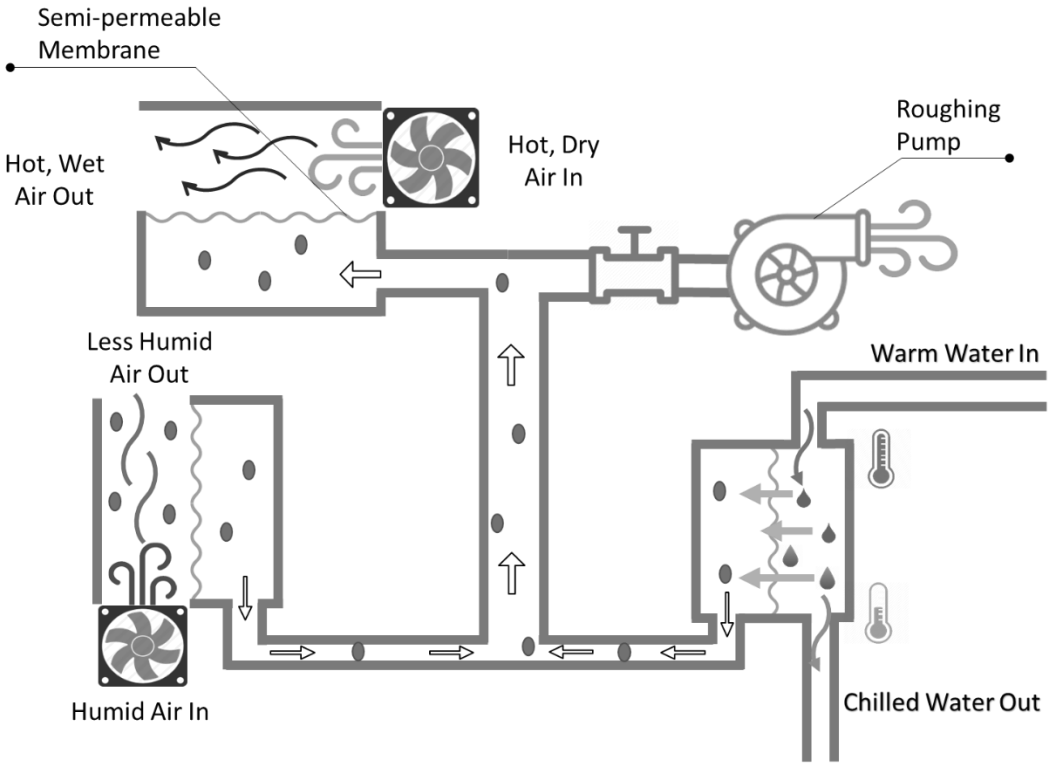

Figure 7: Thermally driven latent and sensible membrane cooling system

2.4 Mass Transfer Characterization

The performance of a membrane module in an MHP is primarily dependent upon the membrane material used and the conditions that promote mass transfer within the channels. The ideal permeation for water vapor though a membrane consists of two different resistance regimes that contribute to the total resistance through a membrane. The resistance between the bulk mean

fluid concentration and the boundary layer concentration at the membrane surface is the interfacial or convective mass transfer resistance. The resistance in this regime is affected by the convective properties of the flow stream, such as Reynolds number, Schmidt number and Sherwood number. The resistance associated to the water vapor transfer through the membrane is known as membrane diffusion resistance. These regimes are depicted in Figure 8.

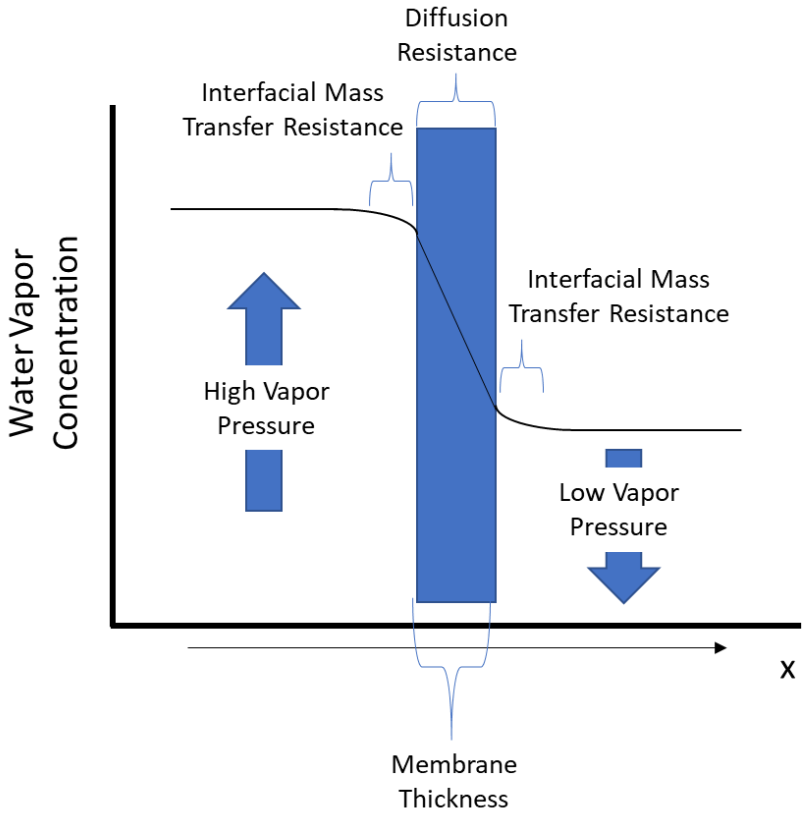

Figure 8: Ideal 1D water permeation

Properly characterizing membranes for their resistance is imperative for developing mass transfer models and for designers of an MHP. This section will focus on a few of the published mass transfer characterization methods.

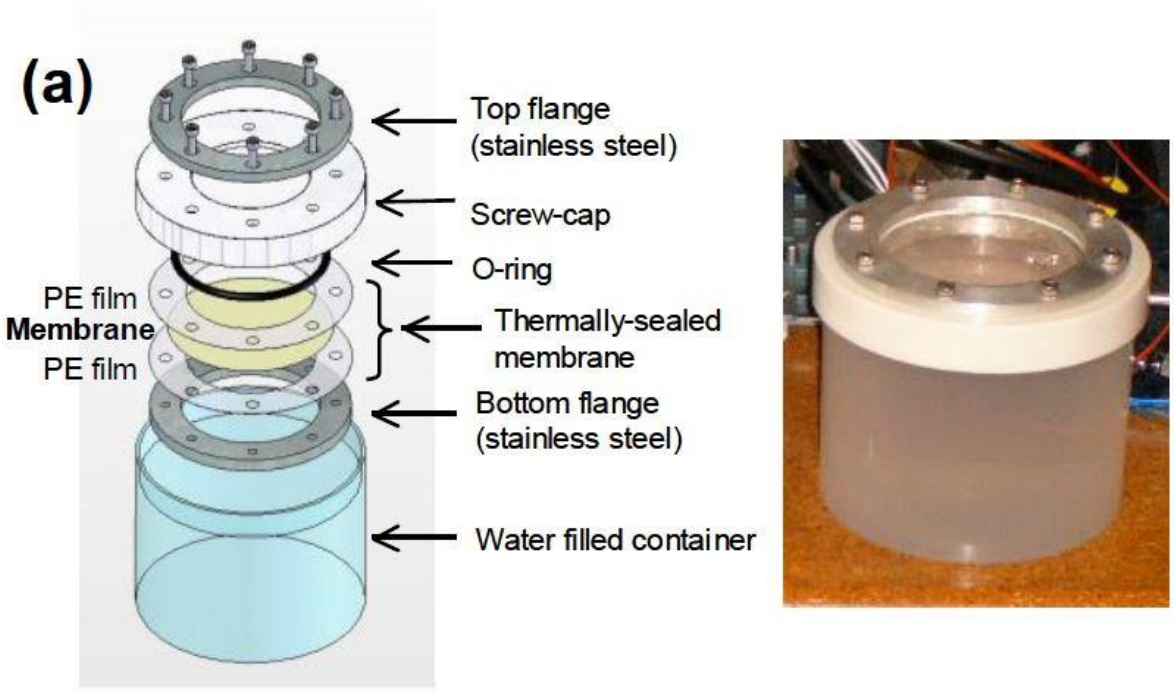

Figure 9: Membrane fixture for vapor permeation experiment by Makota [25]

Makoto evaluated water vapor transfer rates by using a cup filled with water that was covered by a membrane and placed in environmental chamber which circulated dry air. The membrane fixture can be seen in Figure 9. The experiment was conducted at 70°C and the mass of the cup was captured at intervals of 2-6hrs. The membrane area was 25cm^2. [25]

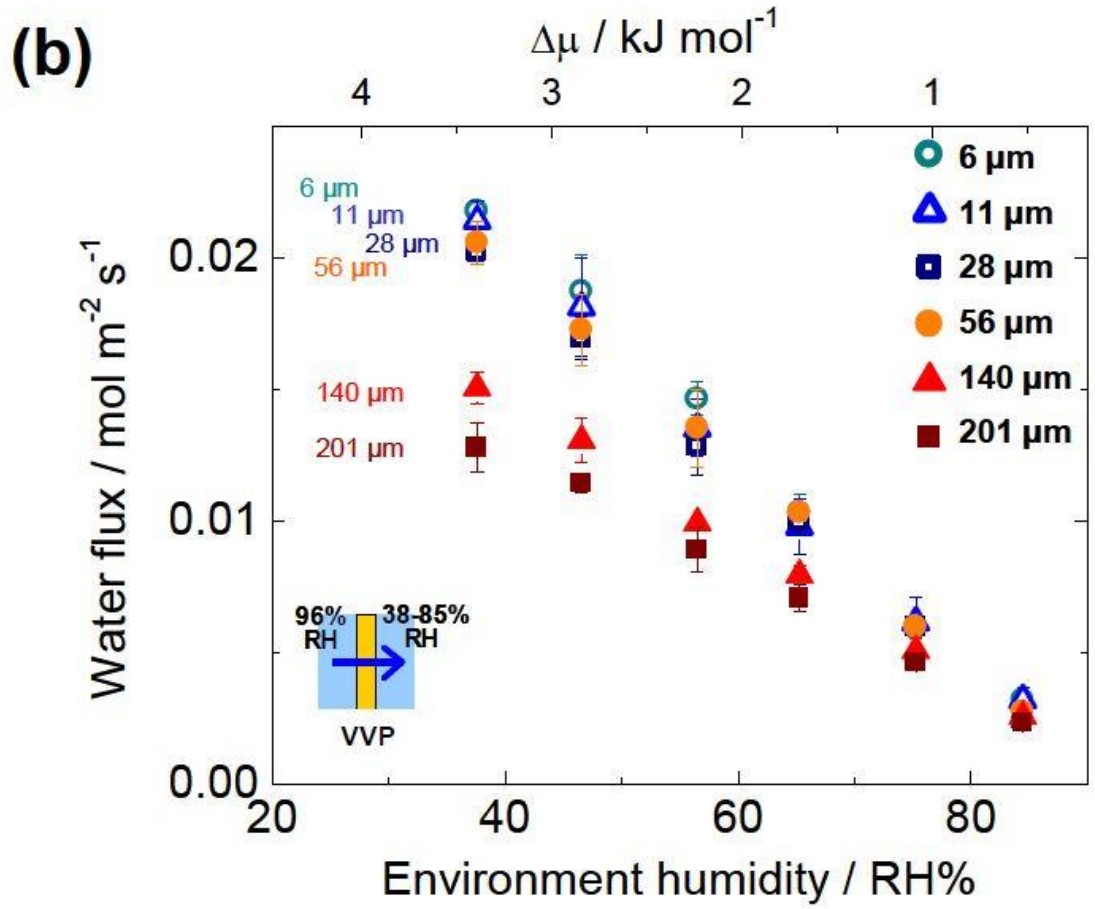

Figure 10: Vapor permeation test results [25]

The results from Makoto's experiment display the effect of the concentration gradient of water vapor across the membranes thickness on transfer rates. The results also show the effect of membrane thickness on mass transfer performance. These relationships follow Fick's Law of diffusion. As shown in Figure 10, the water vapor flux is directly proportional to the change in water vapor concentration across the thickness of the membrane.

Majsztrik et al. used the analysis in Figure 11 to flow dry Nitrogen and humidified Nitrogen on either side of a 1cm^2 test cell. RH was measured at each inlet and outlet to determine rate of

mass flux rate through the system at 30 °C. The materials tested included varying thicknesses of a Perfluoro Sulfinated Acid (PFSA) membrane. [26]

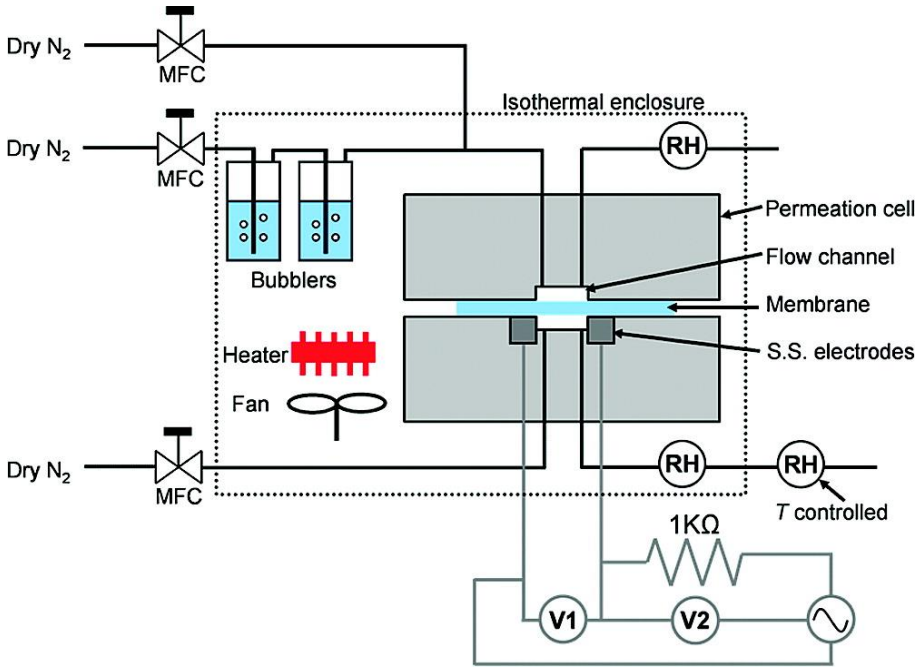

Figure 11: Testing assembly used by Majsztrik [26]

The results from the experiments are seen in Figure 12. As the flow rate into the test cell increases the mass flux through the membrane increased. Additionally, as the flow rate increases the controlling resistance changes from convection limited to diffusion limited. At low flow rates, the membrane can remove water vapor from the supply air at the same rate that water vapor is delivered to the test cell. As the flow rate is further increased, more water vapor is delivered to the membrane than what the membrane can remove. At this point the rate of mass flux increases in a linear manor and the resistance from diffusion is the primary contributor to the mass flux.

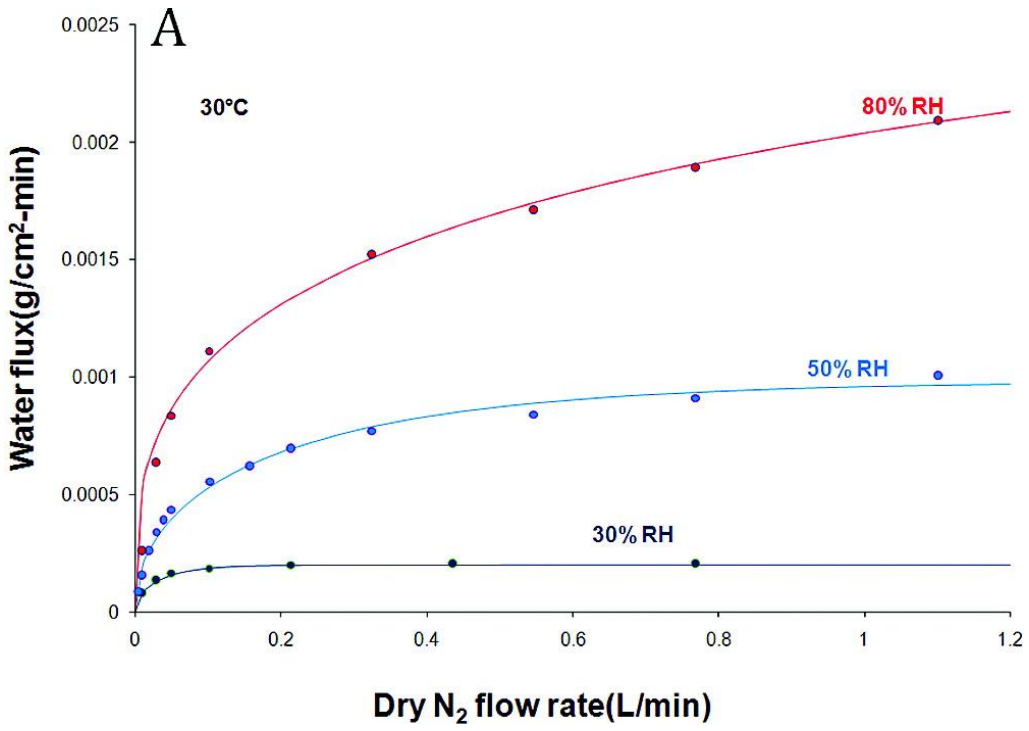

Figure 12: Water vapor flux as a function of Nitrogen flow rate at 30°C [26]

The study by Majsztrik et al. displays the resistance regimes that effect mass transfer as flow rate is varied, however the study was not focused for the HVAC applications. To date, many studies have published results on various membranes and diffusion rates, yet little research has been published on the convective mass transfer resistance in a membrane mass exchanger specifically for HVAC applications.

2.5 Materials

Membranes have been used for many applications such as gas separation, desalination, biomedical, energy recovery, etc. There are two types of membranes used for water selection, porous and homogeneous. Porous membranes are typically used for filtering applications with pore sizes only large enough for water to permeate while larger molecules cannot penetrate. Homogeneous membranes are ideal for membrane heat pumps due to their high-water selectivity.

There are numerous homogeneous polymer membrane materials currently being investigated for water transfer applications by various research groups around the world. Many of these materials are experimental with no near-term viable path to high volume production. To this end, there are numerous hydrocarbon materials that were considered as these are more readily produced. As shown in Figure 13, most of these materials have poor water selectivity and permeability. In the few published studies on their durability, it is shown that hydrocarbon membranes fail quickly relative to perfluorinated materials. [27]

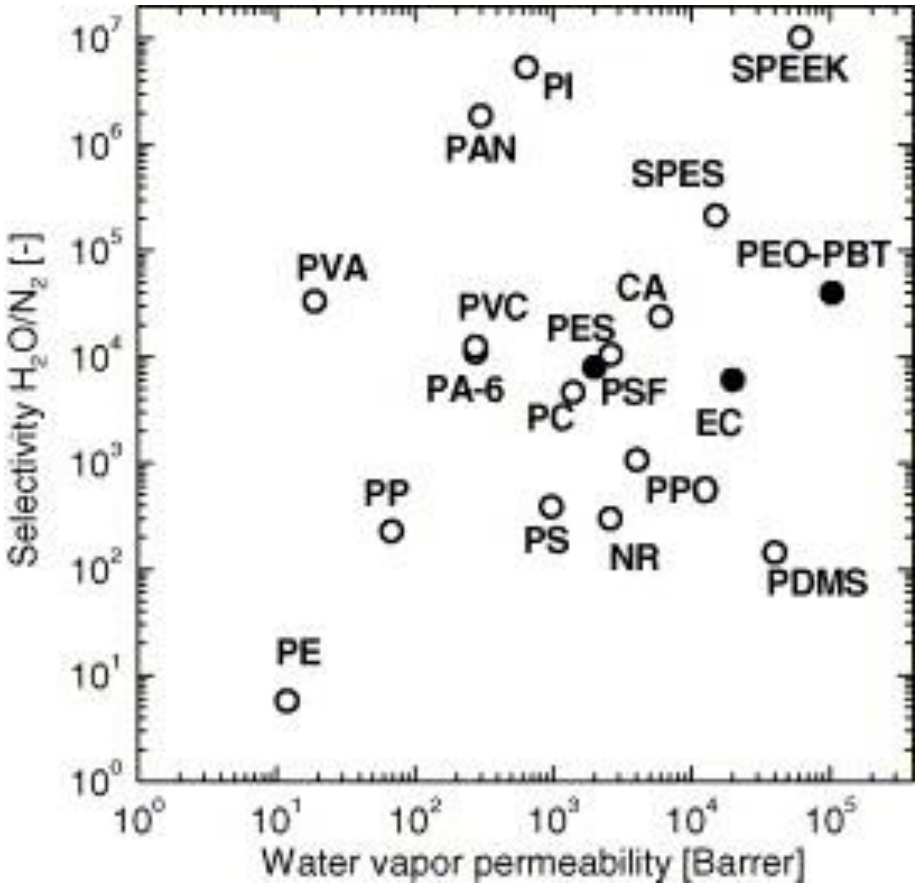

Figure 13: Hydrocarbon membrane performance [6]

Most common membranes and membrane laminates of interest are seen in the list below and in Figure 14 and Figure 15:

- Microporous PTFE membrane or microporous polytetrafluoroethylene membrane consists of a textile fabric with a membrane laminate. These are resistant to liquid water mass transport, however there is little resistance for water vapor diffusion. This selectivity is due to the microporous structure and the hydrophobic surface properties of the PTFE. [4]
- Perfluoro sulfonate ionomer membrane (PFSA) is a commonly produced membrane often found in use for Proton Exchange Membrane fuel cells with the commercial name Nafion®. The transport of water and water vapor within this membrane occurs due to electro-osmotic drag or by diffusion gradient. [28]
- Polymer membranes and Polymer membranes laminates are a polymer membrane that act as a liquid barrier yet still allow water vapor transport. These are typically used in clothing to enable the pass through of water vapor such as sweat. Some of the commercial names of these materials include Gore-Tex® and Sympatex® [8,29].
- Derivatized cellophane membranes are typically used in the medical field and for food packaging due to their low permeability rates and are made of cellulose [4].

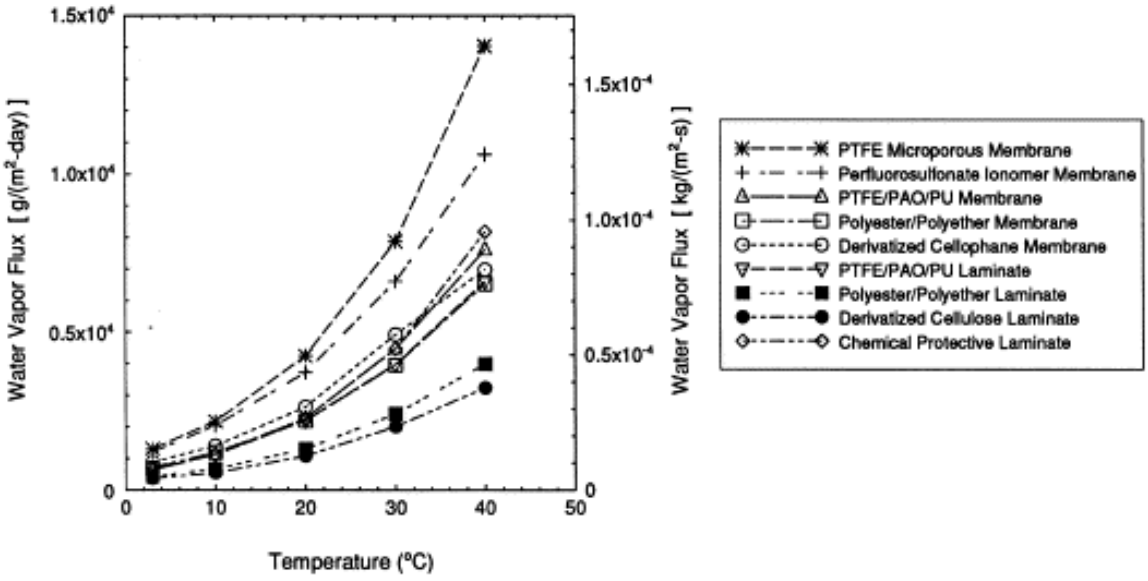

Figure 14: Water vapor flux as a function of temperature [4]

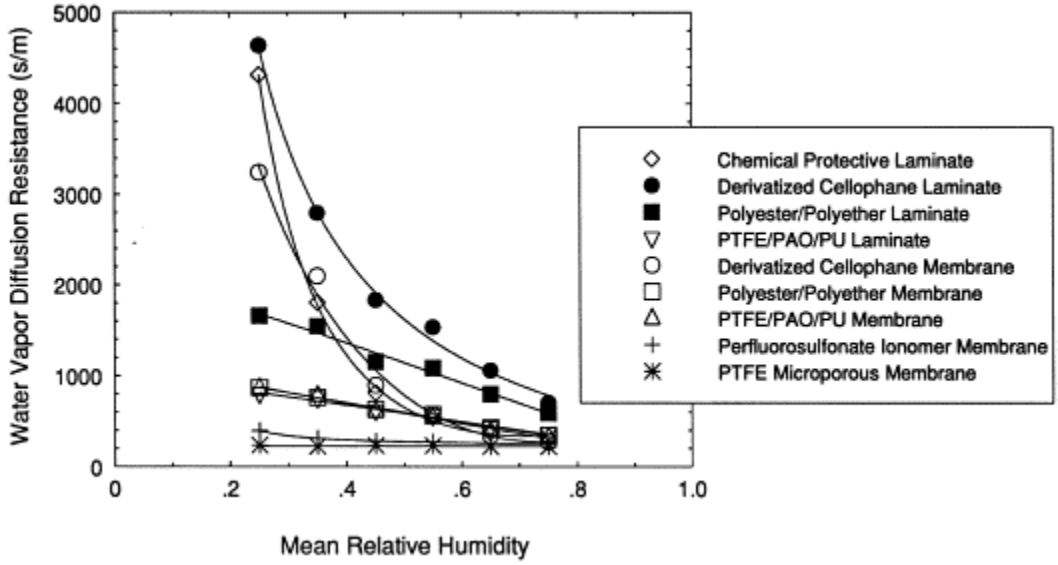

Figure 15: Water vapor diffusion as a function of mean relative humidity [4]

Figure 14 shows the effect that temperature has on the flux. As the temperature increases the water vapor flux increases for each material represents. Additionally, Figure 15 displays that as the mean relative humidity increases the diffusion resistance for each material decreases.

3. Experimental

A set of experiments were developed for the study of convective mass transfer resistance in a membrane mass exchanger for HVAC applications while also provide supporting evidence for a membrane heat pump system that is thermally driven. As a result of these experiments, a series of correlations used to model mass transfer was outlined and advanced hardware and testing equipment was developed.

The experiments consist of two different evaluations. The first evaluation measured mass transfer with a sweep gas. The second evaluation measured mass transfer for a vacuum mass exchanger. The results from the first two experiments were collected and used to validate a down the channel mass transfer model. The validated mass transfer is later used to simulate a 3 rTon MHP DOAS.

3.1 Membrane and Channel Performance Evaluations

The first two evaluations completed were designed specifically for material characterization and channel resistance measurement. The collected results were used to identify the proper correlations for estimating the Sherwood number, and convective resistance while also determining the diffusion coefficient for a PFSA membrane.

3.1.1 Hardware Designs for Membrane and Channel Performance Evaluations

The testing equipment developed required unique designs to enable multiple configurations of flow geometry to be evaluated under the same conditions. All testing systems were built and calibrated to specifically complete the tests outlined in this series of experiments. The testing hardware were constructed in a consistent manor with design considerations for pressure drop, material compatibility, manufacturability, alignment, and flow distribution. The test conditions selected correlate to the current set of conditions placed on HVAC components by ASHRAE pertaining to pressure drop of components and face velocity while also exploring mass exchanger design at high pressure drop to observe the tradeoff of pressure drop and effective latent cooling.

3.1.2 Sweep Gas Experiments

The experimental configurations were designed to specifically investigate membrane water vapor transfer using representative flow conditions and concentration gradients seen in HVAC systems. The first configuration utilized a sweep gas at a controlled humidity with no pressure difference across the membrane. The system schematic is seen in Figure 16. Compressed air is supplied to mass flow controllers for separate wet and dry flow and humidity control. Each flow stream had separate mass flow control, specified by Labiew, to a dryer and humidifier, where air was dehumidified with a granular desiccant and the wet-side air humidified by custom built bubblers at a controlled dew point. A relative humidity sensor was used to control the mixing ratio

on each side at the inlet of the membrane test hardware. Additional relative humidity sensors were used at the outlet to monitor the change in water content of the dry and wet flow through the test section. Temperature and pressure were also monitored at the inlet and outlet of each gas stream.

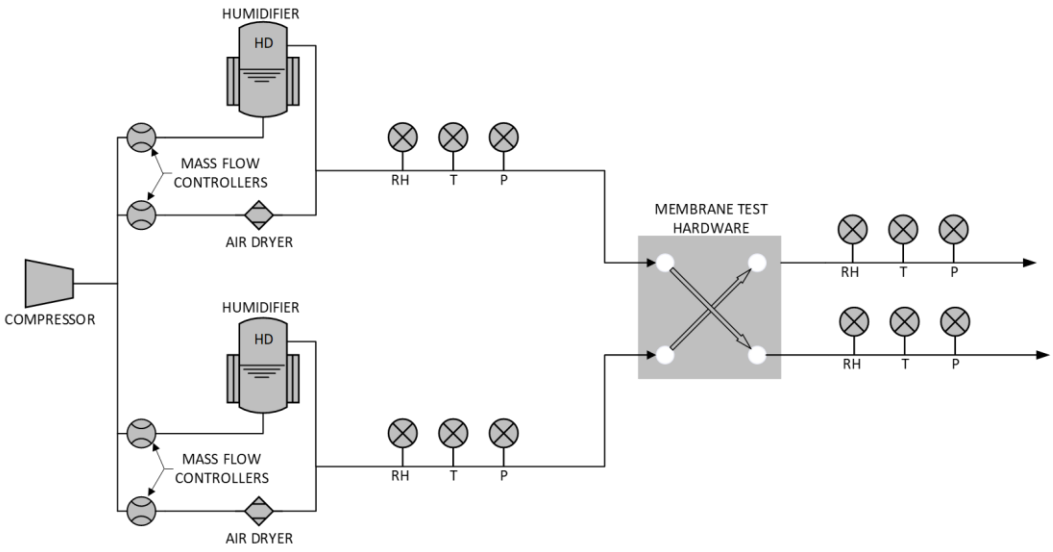

Figure 16: Membrane dehumidification with sweep gas experimental configuration.

3.1.3 Vacuum Pressure Experiments

Another evaluation was completed to observe the resistance of transferring water vapor from an ambient air stream to an all-water sink at a controlled vacuum pressure. The system diagram for the experiment can be seen in Figure 17. Compressed air is supplied to mass flow controllers for the supply air flow and humidity control. Supply air was humidified by custom built bubblers and dehumidified with a granular desiccant. A relative humidity sensor was used to control the mixing ratio at the inlet of the membrane test hardware. Additional relative humidity sensors were used at the outlet to monitor the change in water content of the supply air flow through the test section. For this experiment, the vacuum is maintained at approximately 900Pa. Humidity was measured at both the inlet and outlet of the process air stream.

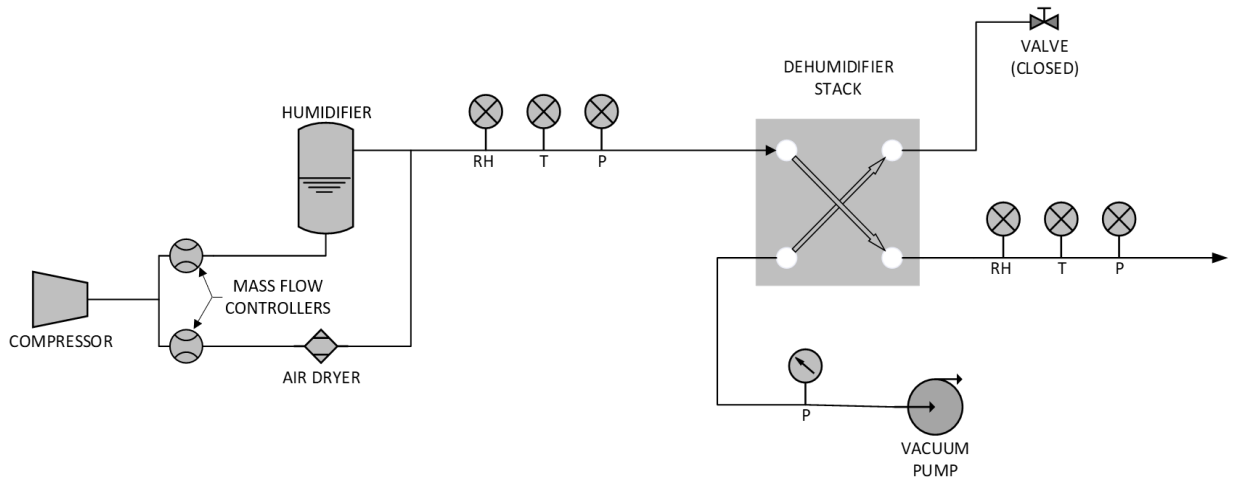

Figure 17: Vacuum Pressure System Diagram

3.1.4 Test Systems

A custom-built test system was developed for the sweep gas experiments and the vacuum pressure experiments and can be seen in Figure 18. The system was capable of controlling gas flow, humidity level for wet and dry air streams, vacuum pump control, and data logging. The specifications for the test stand are given in Table 1. Compressed air is supplied to two Unit 1000 mass flow controllers and two Porter mass flow controllers. After passing through mass flow controllers, air is either dehumidified by a Drierite Laboratory Gas Drying Unit filled with 1lb of indicating desiccant or is humidified by custom built bubblers. Air is then measured by an Omega HX-71 V2 Relative Humidity sensor and a Drok pressure transducer before being delivered to the membrane testing hardware. Temperature and atmospheric pressure were monitored continuously by a BME280 pressure transducer. For vacuum pressure experiments, a SMC vacuum transducer is used to monitor the pressure. An Edwards E2M0.7 rotary vane vacuum pump was used for all required experiments. Data is collected by an Arduino Mega 2560 R3 and is controlled by LabView. For each experiment, a dedicated LabView VI was created. These VI interfaces can be seen in Figure 19 and Figure 20.

Table 1: Sweep gas and vacuum pressure test stand specifications

Control	Specifications
Wet Side Flow	1 – 5 LPM
Dry Side Flow	1 – 5 LPM
Wet Side Humidity	1% - 90%
Dry Side Humidity	1% - 90%
Feed Gas	Air
Logger Rate	1 Hz

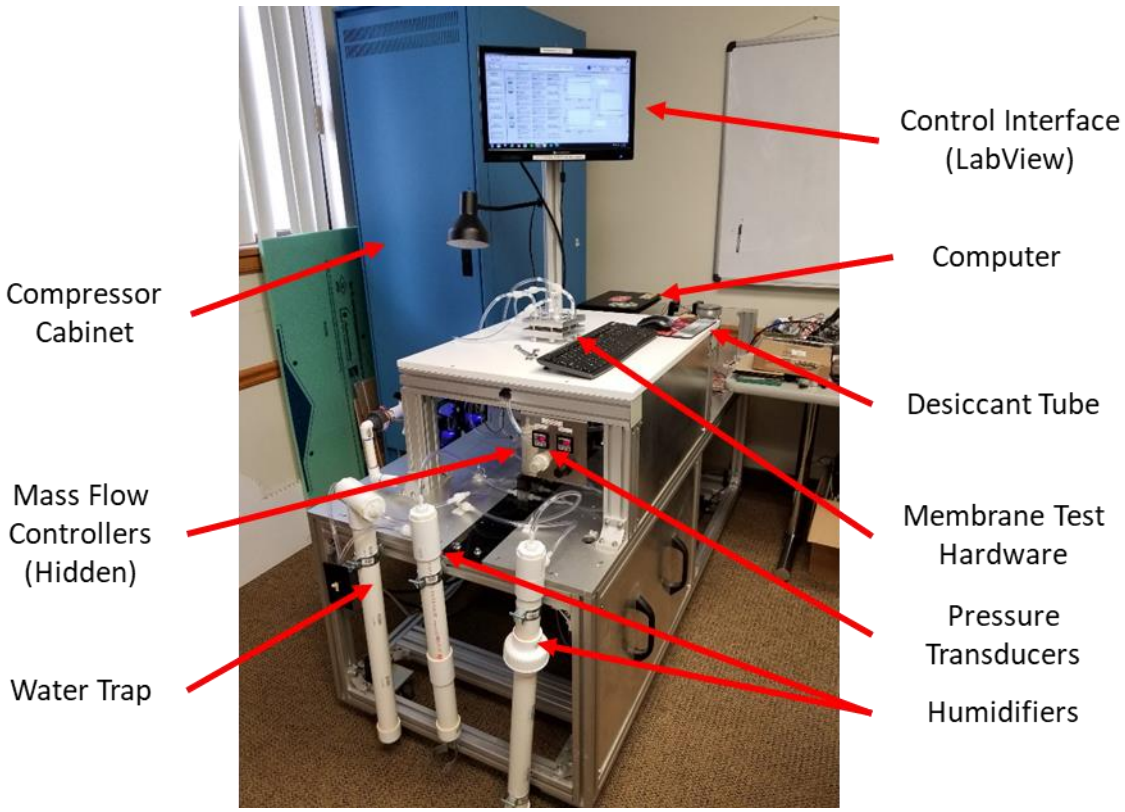

Figure 18: Sweep gas and vacuum pressure test system

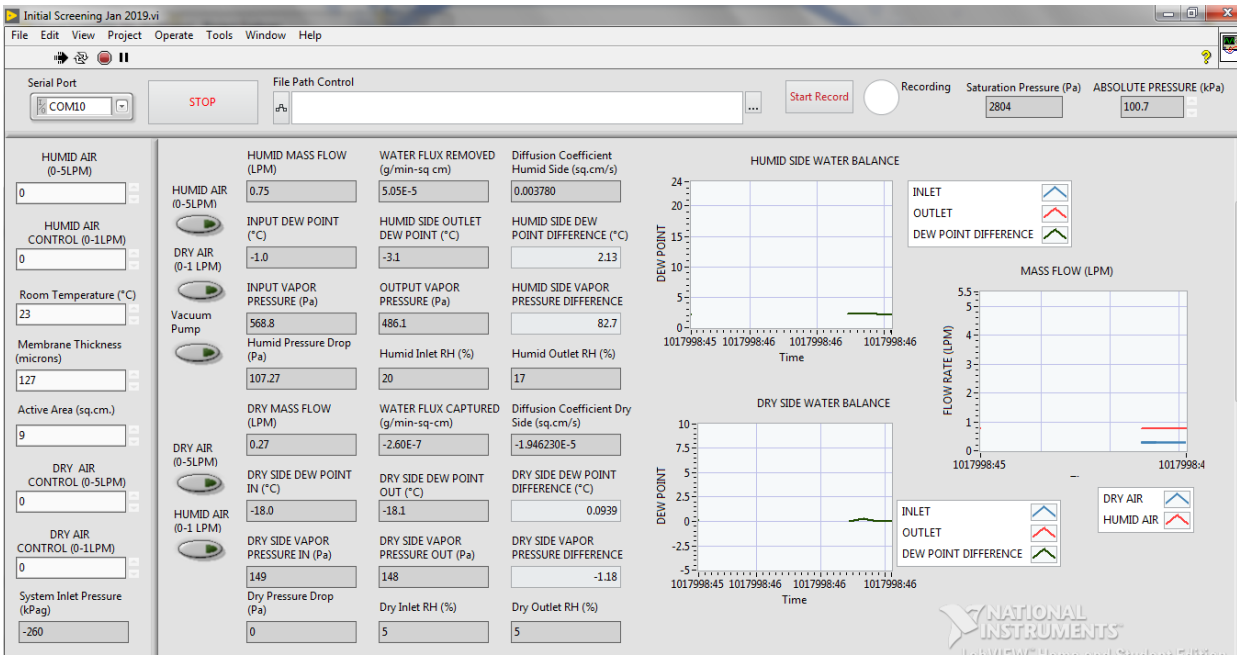

Figure 19: LabView control panel for sweep gas experiments

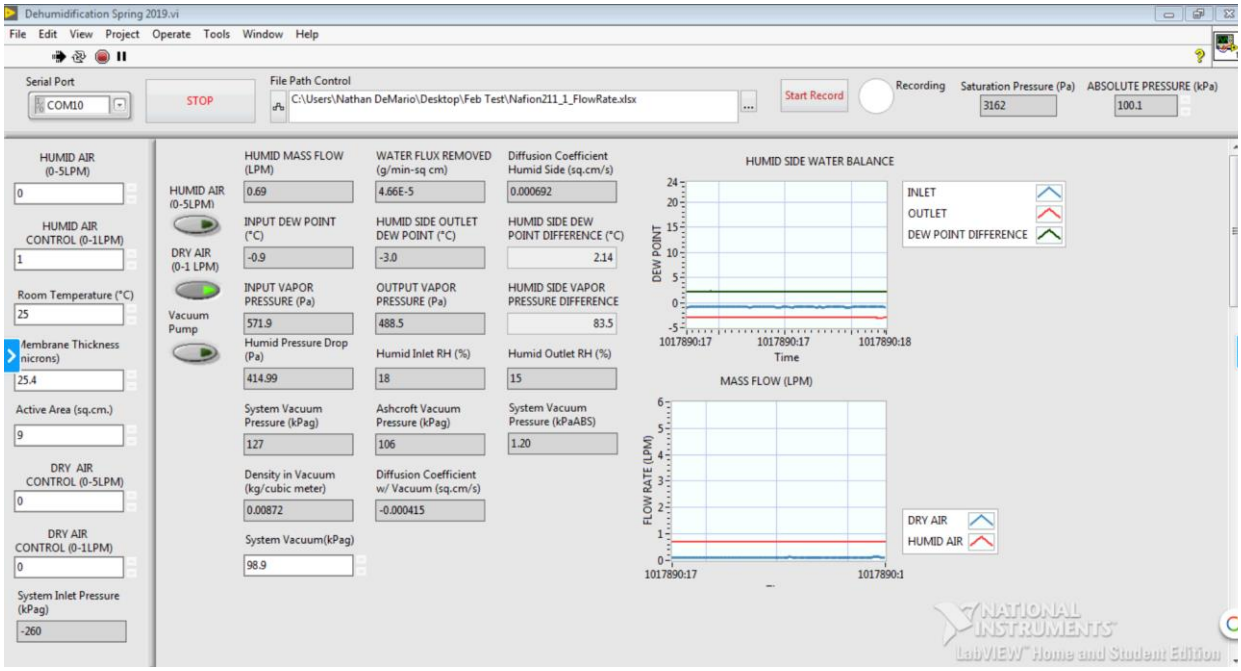

Figure 20: LabView control panel for vacuum pressure experiments

3.1.5 Hardware Assembly

For sweep gas evaluations, a 9 cm^2 flow field made of rectangular channels was used. The channels were 2 mm in width. Channel thickness was varied from 0.5, 1.1, 1.6, and 3.1 mm. Channel geometry can be seen in Figure 21. Flow fields were constructed of 3 layers of laser cut acrylic sheet adhered together. Supplemental views of the flow field and flow field assembly can be seen in Figure 22, and Figure 23. The channel length of the acrylic was 55 mm and was reduced to 45 mm by a polyimide tape layer which was used to make the active area window for the membrane. The acrylic layers were adhered together to create a plate assembly.

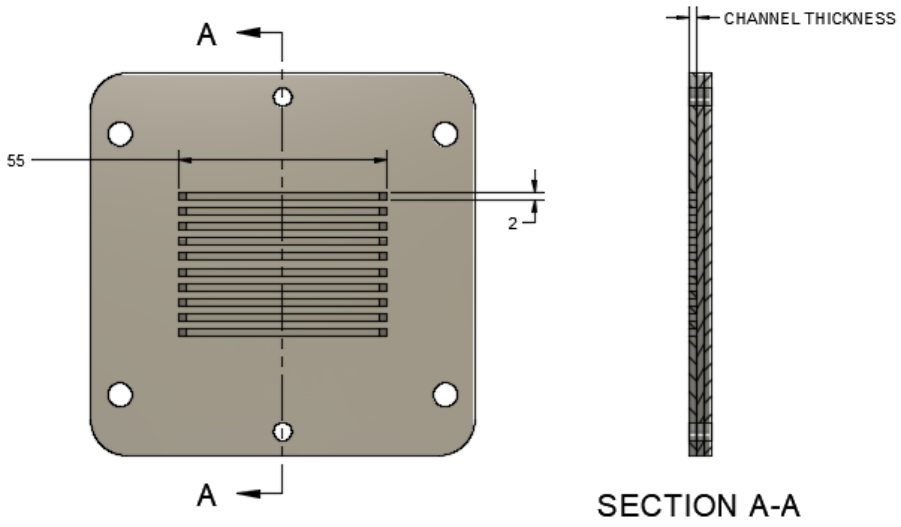

Figure 21: Flow field geometry

PARTS LIST	
ITEM	PART NUMBER
1	BASE LAYER
2	SUPPORT LAYER
3	CHANNEL LAYER

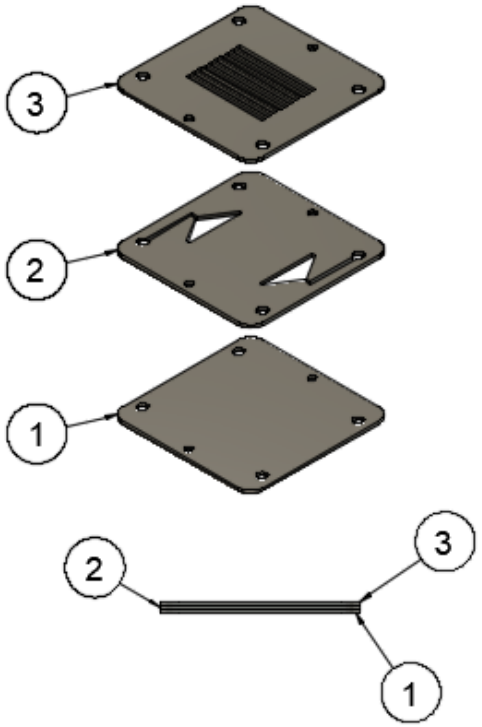

Figure 22: Flow field exploded view

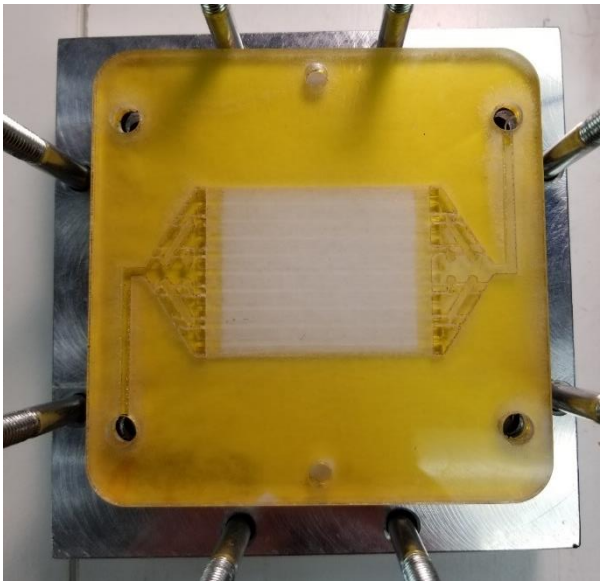

Figure 23: Picture of flow field geometry

The flow field consists of four ports. Two ports guide the wet flow while the other two guide dry air flow. This can be seen in Figure 24. The membrane was placed on top of the channels. A silicone face seal gasket was placed on top of the membrane. Following the membrane, a second flow field geometry was placed with the channel side facing the membrane.

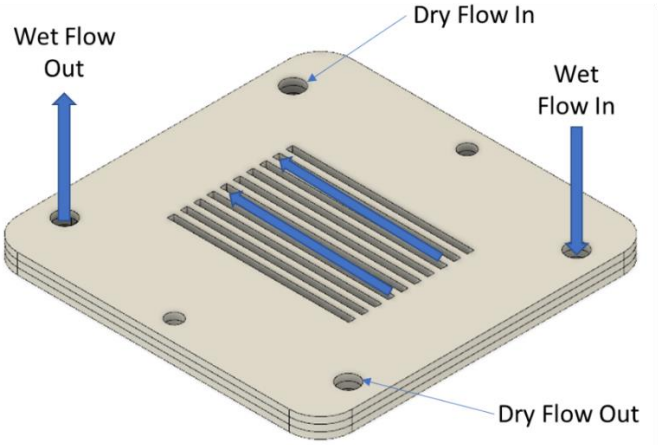

Figure 24: Flow field geometry

End hardware was machined from 6061 Aluminum. Eight bolts were used to provide even clamping force throughout the assembly. Plastic barbed fittings were used to connect the end hardware to the test stand. O-rings were used at each port to create a seal between the end hardware and the flow field geometry. The flow fields are assembled such that both feed flows passed through the channels in the same direction. A picture of the assembly can be seen in Figure 25.

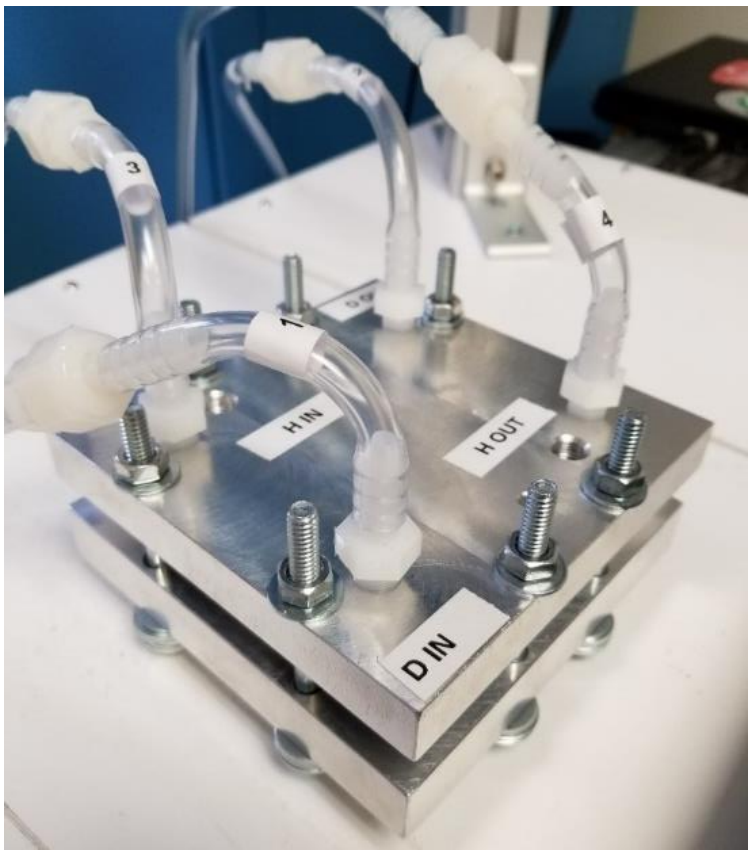

Figure 25: A picture of the vapor driven hardware assembly

For vacuum pressure experiments, the same $9cm^2$ flow field geometry was used as previously described for the supply air. The vacuum side plate was comprised of an embedded porous plastic in a custom-made membrane support structure. The vacuum side assembly can be seen in Figure 26 and Figure 27. Acrylic layers were again bonded together to create the frame of the membrane support structure.

PARTS LIST	
ITEM	PART NUMBER
1	BASE LAYER
2	SUPPORT LAYER
3	BOUNDARY LAYER
4	POROUS PLASTIC

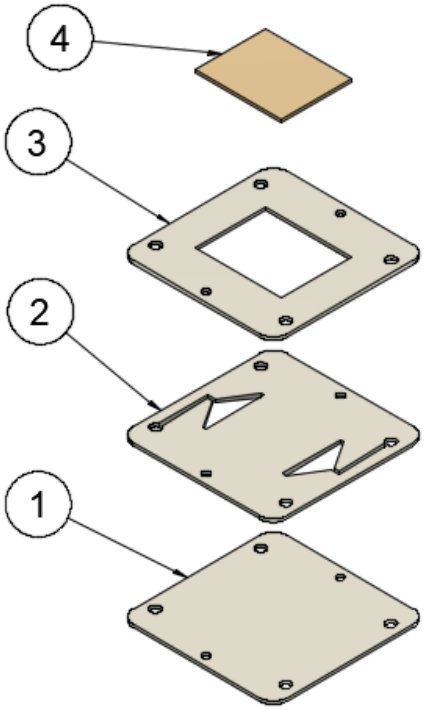

Figure 26: Exploded view of the membrane support assembly

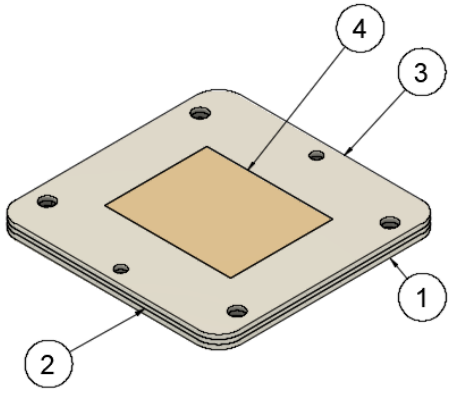

Figure 27: Membrane support assembly

To create a sealed environment between the flow field assemblies, a silicone face seal gasket was used. The membrane was layered in between the porous membrane support with the gasket and flow field. This assembly can be seen in Figure 28.

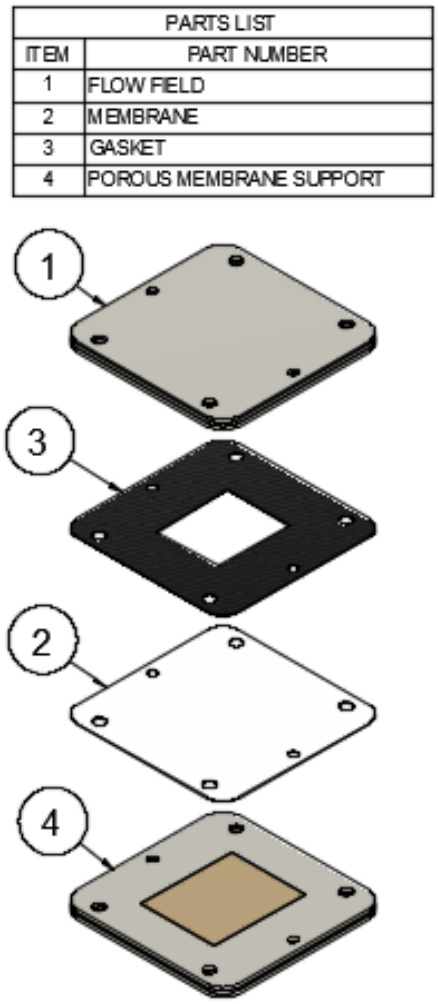

Figure 28: Exploded view of the vacuum pressure test hardware

Aluminum end hardware was used to connect the acrylic flow field and porous membrane support to the test stand. Brass hardware, compression fittings, and vacuum rated refrigeration tubing were used to allow the vacuum to communicate with the aluminum manifold and can be seen in Figure 29.

Figure 29: A picture of the vacuum pressure hardware assembled.

3.1.6 Calibration

All controllers and sensors were calibrated to ensure accurate measurements of water vapor. Mass flow controllers were calibrated using an Alicat Scientific calibration box to +/-0.02 SLPM. Pressure transducers were calibrated by a digital monometer which was integrated within the Alicat Scientific to +/- 10 Pa, and RH sensors were calibrated using the dew cup method. The ambient pressure and temperature were monitored by a factory calibrated BME280 to +/-1 Pa and +/- 1°C, respectively.

3.1.7 Test Plan

A consistent set of parameters were used to complete each set of experiments. The test hardware was assembled in the same manor for each configuration. The testing parameters that were used to complete the sweep gas experiments can be seen in Table 2. The channel depth was varied at 0.5, 1.1, 1.6, and 3.1 mm. For each channel depth the inlet RH was maintained at 80% and 20%. The feed rate of air was set to 1, 2, 3, 4, 5 standard liters per minute (SLPM) for each

channel depth. Data was logged at 1Hz. For vacuum pressure experiments, the testing parameters can be seen in Table 3. The channel depth was varied at 0.5, 1.0, and 2.0 mm. The inlet relative humidity was maintained at 80% for flow rates of 1, 2, 3, 4, 5 SLPM. The vacuum pressure was 900 Pa.

For the studies presented, perflourosulfinated acid (PFSA) ionomer membranes were used at varying membrane thicknesses of 25, 50, 130, and 180 microns. The cast membranes were used as received in proton form. PFSA was chosen for these benchmark experiments because it is reported to have the lowest resistance to water vapor transfer and high water selectivity [4,26,30]. From a performance perspective, PFSA is thought to represent the best commercially available polymer for homogeneous water transfer membranes.

Table 2: Testing parameters for sweep gas experiments

Parameter	Value
Active area	9 cm^2
Channel depth	0.5, 1.1, 1.6, 3.1 mm
Feed gas	Air
Temperature	23.5 °C
Wet feed total pressure	~1 atm
Dry feed total pressure	~1 atm
Wet feed RH	80%
Dry feed RH	20%
Wet feed rate	1,2,3,4,5 SLPM
Dry feed rate	1,2,3,4,5 SLPM

Table 3: Testing parameters for vacuum pressure experiments

Parameter	Value
Active area	9 cm^2
Channel depth	0.5, 1.0, 2.0 mm
Feed gas	Air
Temperature	23.5 °C
Wet feed pressure	~1 atm
Low pressure	0.9 kPa
Wet feed RH	80%
Wet feed rate	1,2,3,4,5 SLPM

4. Results and Discussion

The observed results are presented from specifically chosen methods that best represent the hypothesis and conclusions that are to be discussed. The presented results are followed by discussion and conclusions.

4.1 Membrane Thickness and Flow Gap Study

The test system described in Section 3.1 was used to observe the mass transfer of four different membranes when evaluated in two different experiments for multiple channel depths. The inlet and outlet RH were measured at 1hz for 30 seconds. The collected data was averaged for each input condition. The test parameters outlined in Table 2 and Table 3 were used for the evaluations.

In all experiments, the RH at the inlet and outlet was used to determine the mass of water removed from the process air flow stream and mass flux j was calculated using Equation 1. Where $\dot{V_{air}}$ is the volumetric flow rate of process air, ρ_{air} is the density of the air, $\Delta\omega$ is the change in humidity ratio of the process air stream, and A is the membrane area.

Equation 1

$$j = \frac{\rho_{air}\dot{V_{air}}\Delta\omega}{A}$$

The measured mass flux at varying process air velocities for all sweep gas and vacuum pressure experiments are given in Figure 30 and Figure 31. Experimental error associated with flow control and the measurement of RH, pressure, and temperature was estimated to be 0.3 mg cm^{-2} min^{-1}. This error was estimated based on the average discrepancy between the sweep and process gas mass balance that was calculated for all sweep gas experiments. The data Figure 30 and Figure 31 demonstrate how both membrane thickness and process gas Reynolds number impacts water vapor transfer. For sweep gas experiments, the mass flux was measured from the

wet flow stream. An increase in vapor flux was observed as the Reynolds number within the channel was increased. Additionally, the observed flux increased as the thickness of the membrane decreased when comparing the flux for each thickness at similar Reynolds numbers. For the analysis, Reynolds number was calculated as follows where velocity is represented by V_{air} in the channel, H_d represents for hydraulic diameter of the channel, and μ represents the dynamic viscosity.

Equation 2

$$Re = \frac{\rho_{air} V_{air} H_d}{\mu}$$

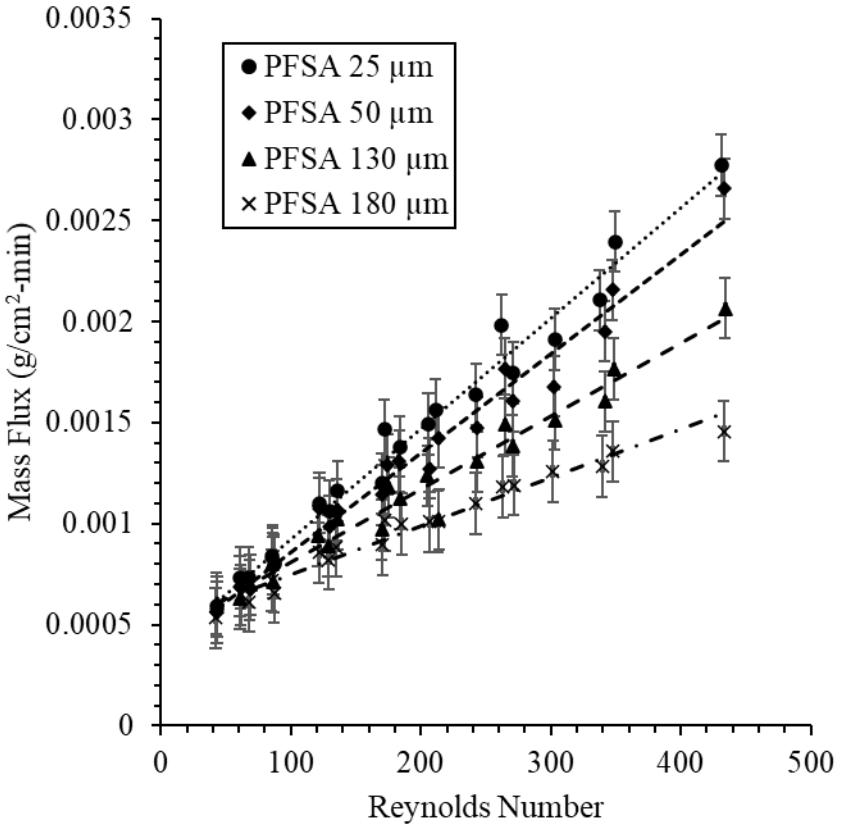

Figure 30: Observed mass flux from sweep gas experiments as Reynolds Number was increased for four different thicknesses of a PFSA membrane.

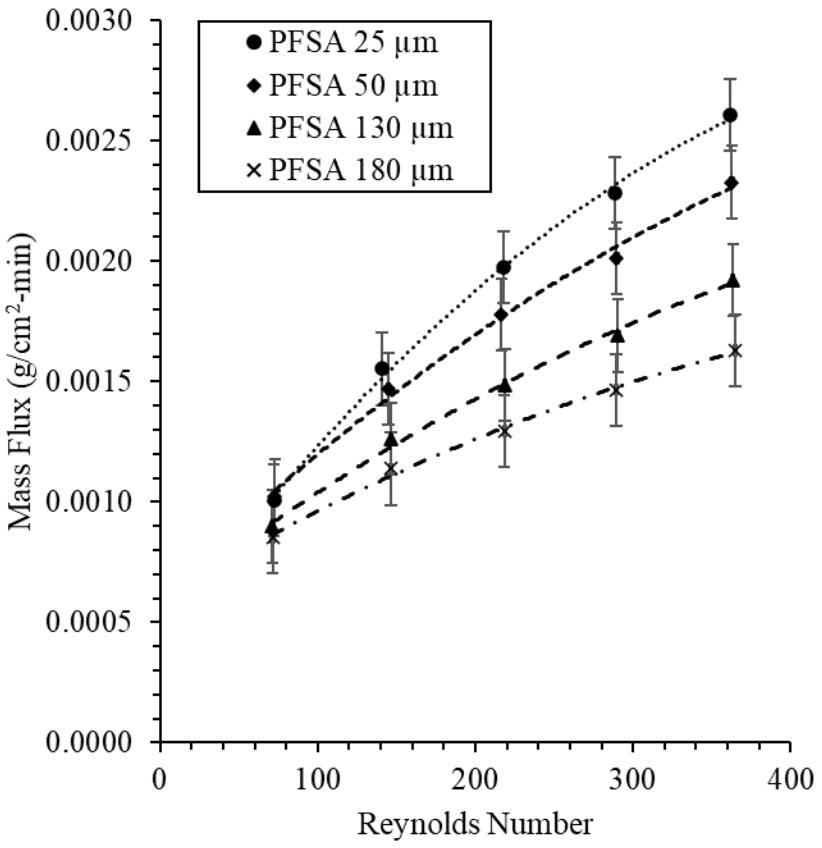

Figure 31: Observed mass flux from vacuum pressure experiments as Reynolds Number was increased for four different thicknesses of a PFSA membrane.

4.1.1 Extraction of Diffusion Resistance and Convective Resistance

Using the data previously presented, an analysis was developed to separate the relative influence of these key parameters. The total mass transport resistance (R_T) for water vapor is the sum of diffusive resistance through the membrane and convective resistance in the channel. While many factors impact the diffusion resistance of a membrane such as temperature, water activity in the polymer, and conductivity, this applied study probes the effective diffusivity (D_{eff}) at steady state for water concentrations and temperature associated with HVAC operating conditions. This enables the relative influence of channel design and flow conditions on the convective mass transfer coefficient (k) to be investigated. Based on the difference between the average

concentration (ΔC) of the wet and dry sides of the membrane and the measured water flux, the total resistance to water transfer is expressed as:

$$j = \frac{\Delta C}{R_T} = \frac{\Delta C}{\frac{t_{mem}}{k_{diff,eff}} + \frac{1}{k_{conv}}} \qquad \textit{Equation 3}$$

In Equation 3, ΔC represents the average change in vapor concentration across the membrane thickness, R_T represents the total resistance, t_{mem} is the thickness of the membrane, $k_{diff,eff}$ is the diffusion coefficient for the material, and k_{conv} is the combined convective resistance of the channels.

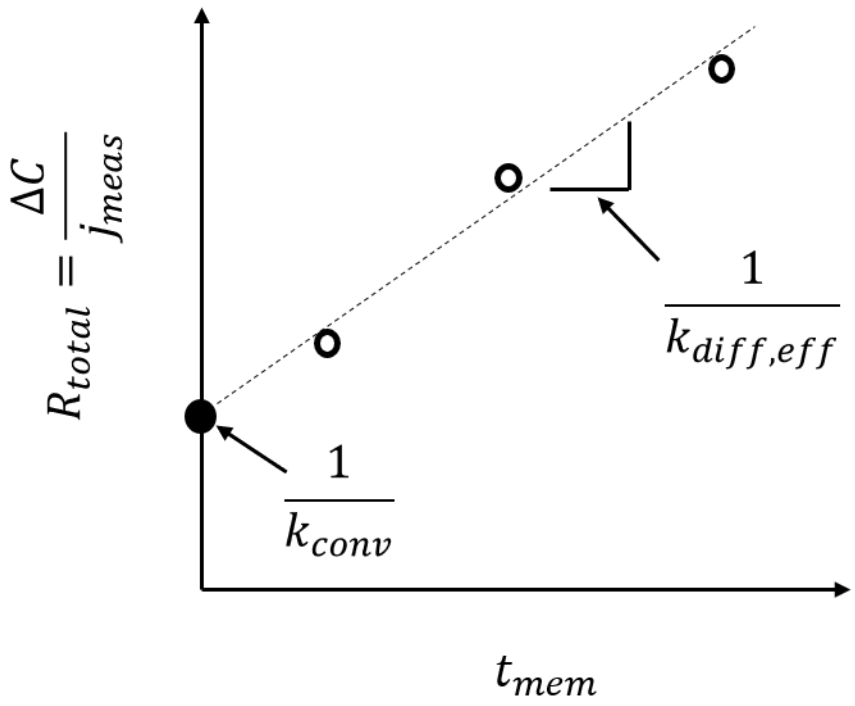

Figure 32: Data analysis to separate convective and diffusive resistance.

As illustrated in Figure 32, the experimental results were organized with total transport resistance as a function of membrane thickness. A linear trend represents a constant diffusivity through the membrane where the slope indicates the diffusion resistance and the intercept represents the convective resistance for a given experimental configuration. Figure 33 displays

this analysis at selected gas velocities. The sweep gas experiment results display channel resistance increases as channel depth increases. As membrane thickness increased, diffusion resistance increased and as flow rate is increases, convective resistance decreases. The data was fitted to a linear regression where the slope and y – intercept was determined. A sufficient coefficient of determination was found with the linear fit yielding an average of 97%.

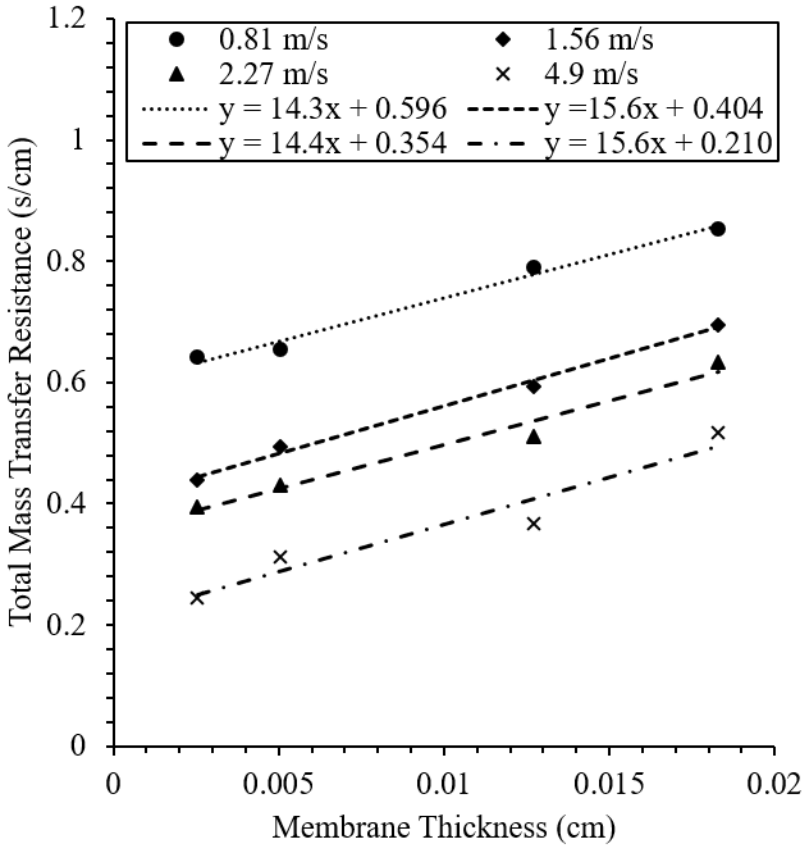

Figure 33: Total diffusion resistance with varying PFSA membrane thickness at increasing gas velocity.

The convective mass transfer resistance is expressed in similar manor to convective heat transfer. In the convective heat transfer expression, Equation 4, the heat transfer rate is represented by $\dot{Q}$, the area of heat transfer is represented by A, the convective mass transfer coefficient is seen as h_{conv}, and the difference in thermal energy between two states is seen as ΔT. Similarly, in the

convective heat transfer expression, Equation 5, the rate of mass transfer is denoted by $\dot{J}$, the area of mass transfer is represented by A, the convective mass transfer coefficient is seen as k, and the difference in species concentration energy between two states is seen as ΔC.

Convective Heat Transfer Expression:

$$\dot{Q} = h_{conv} A \Delta T \qquad \textit{Equation 4}$$

Convective Mass Transfer Expression:

$$\dot{J} = kA\Delta C \qquad \textit{Equation 5}$$

Several correlations have been published in literature that allow for convective resistance to be predicted. In the governing expressions relating to heat and mass transfer, properly characterizing the convective resistance term requires using various mass and heat transfer supporting expressions. For mass transfer, this includes fluid's density, velocity, dynamic viscosity, momentum diffusivity, mass diffusivity, and the hydraulic diameter of the flow geometry. The Reynolds number is used to characterize the type of flow within the channel as a function of the fluid's density, velocity, dynamic viscosity, and the hydraulic diameter. The Schmidt number describes the ratio of momentum diffusivity (D_{AB}) and mass diffusivity of the fluid to characterize momentum and mass diffusion in the gas velocity and boundary layer.

The Sherwood number is used to characterize the effectiveness of mass convection at the boundary layer of the membrane. Equation 6 presents a correlation for the Sherwood number for Prandtl number that is greater than 0.6 and for Reynold numbers less than $5 \cdot 10^5$. The Reynolds number is represented by Re and the Schmidt number is presented as Sc:

$$Sh = 0.332Re^{1/2}Sc^{1/3}\ [31] \qquad \textit{Equation 6}$$

Using the Sherwood number, an estimated convective mass transfer coefficient is determined from Equation 7 where H_d is the hydraulic diameter and D_{AB} is the mass diffusivity of water vapor in air.

$$k_{conv} = Sh\left(\frac{D_{AB}}{H_d}\right) \qquad \textit{Equation 7}$$

The experimentally determined mass transfer resistance is used to validate the empirical correlation given in Equation 6. Figure 34 compares the observed channel resistance to the empirical correlations as a function of the in-channel Reynolds number.

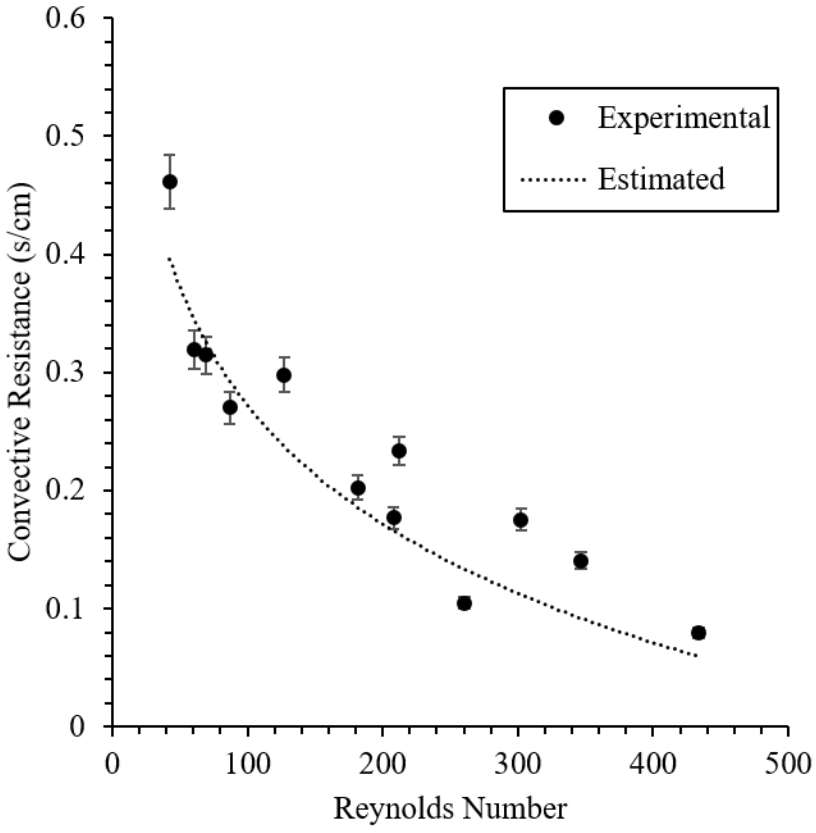

Figure 34: A comparison of the experimental and estimated convective resistance as a function of the Reynolds Number.

Table 4 contains the measured diffusion coefficient, diffusion resistance and convective resistance for each membrane and channel configuration evaluated. The measured diffusion coefficient was used to find the diffusion resistance for each PFSA membrane observed.

Table 4: Observed diffusion resistance and convective resistance from sweep gas experiments

Gas Velocity	Diffusion Coefficient	Diffusion Resistance				Convective Resistance
		PFSA 25 µm	PFSA 50 µm	PFSA 130 µm	PFSA 180 µm	
m/s	cm^2/s	s/cm	s/cm	s/cm	s/cm	s/cm
0.3	0.15	0.02	0.03	0.08	0.12	0.46135
0.5	0.07	0.04	0.07	0.18	0.25	0.31935
0.8	0.09	0.03	0.06	0.14	0.21	0.3148
0.8	0.07	0.04	0.07	0.18	0.26	0.298
1.3	0.05	0.05	0.09	0.23	0.33	0.23345
1.6	0.06	0.04	0.08	0.20	0.29	0.20235
1.6	0.10	0.03	0.05	0.13	0.18	0.27035
2.3	0.07	0.04	0.07	0.18	0.26	0.17675
2.6	0.06	0.04	0.08	0.20	0.29	0.17555
3.8	0.06	0.04	0.08	0.21	0.30	0.1405
4.9	0.06	0.04	0.08	0.20	0.29	0.1049
8.2	0.06	0.05	0.09	0.23	0.33	0.0796

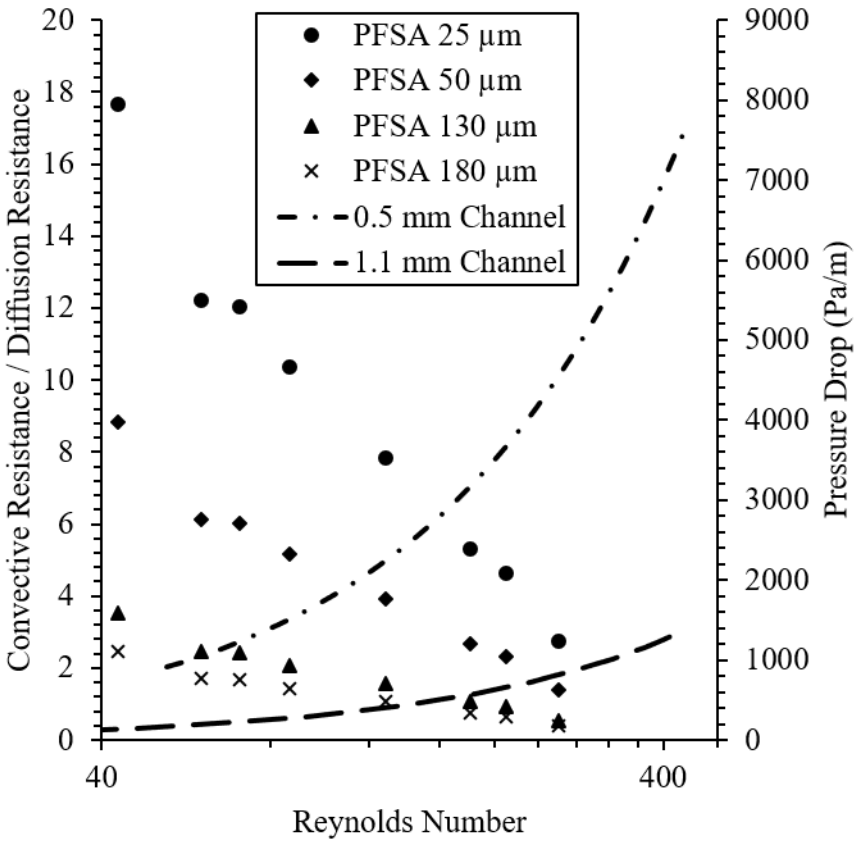

Figure 35: A comparison of the convective resistance to the diffusion resistance as gas velocity increases in the channel for four PFSA membranes. Additionally, the pressure drops incurred within the channel for each channel depth is displayed as a function of gas velocity.

Figure 35 compares the convective resistance over the diffusion resistance as a function of membrane thickness and Reynolds number while also displaying the pressure drop in the channel as a function of channel length. It is seen that channel convective resistance is significantly greater than diffusion resistance for the evaluated PFSA membranes, especially for membranes less than 100 µm in thickness. To reach a convective resistance that is equal to the diffusion resistance, a Reynolds number around 400 would be required.

4.2 Applying Results to a One Dimensional, Down the Channel, Mass Transfer Model

To predict in-channel conditions for mass transfer, a model was developed from Equation 3 that evaluates the rate of mass transfer along the axis of the channel. The model was developed starting with an individual channel and creating a computational grid. A visual representation of the computation model can be seen in Figure 36.

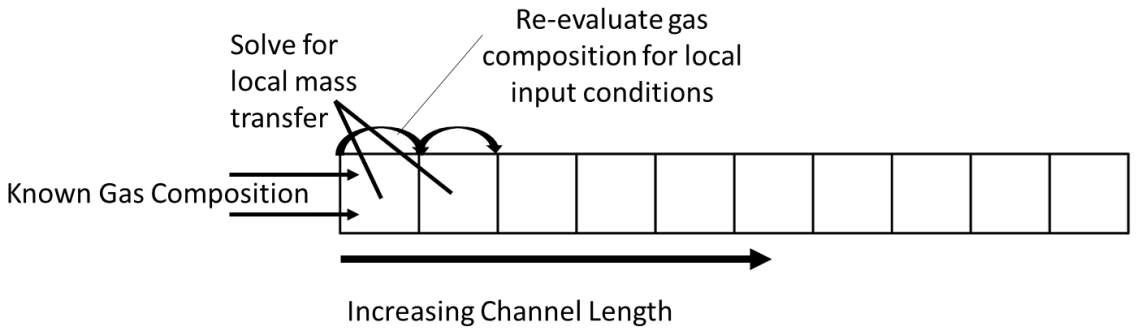

Figure 36: A graphical depiction of the computation domain used to develop the 1D, down the channel, mass transfer model.

The validated empirical correlations given earlier are used to determine the convection resistance based on the channel dimensions and flow rate. The observed diffusion coefficient of the PFSA membrane was used to determine the diffusion resistance. The input conditions of the gas entering have a known 3.1mm which are used to determine the local concentration of the water vapor in the stream(s). The mass flux is then calculated at every 0.01 cm throughout the channel yielding 450 components to complete an analysis for one 45 mm channel. The amount of water vapor that is removed or added, is used to adjust the respective streams' local concentration for the next section in the computational domain. To simulate vacuum experiments, it was assumed that the convective resistance within the vacuum plenum was negligible and the water vapor concentration was constant at 900 Pa.

A comparison of the simulated outlet humidity ratio to the observed outlet humidity ratio can be seen in Figure 37 for a channel with a depth of 3.1 mm for sweep gas experiments. In addition, a comparison of the simulated outlet humidity ratio to the observed outlet humidity ratio for a channel depth of 3.1 mm for vacuum experiments is displayed by Figure 38.

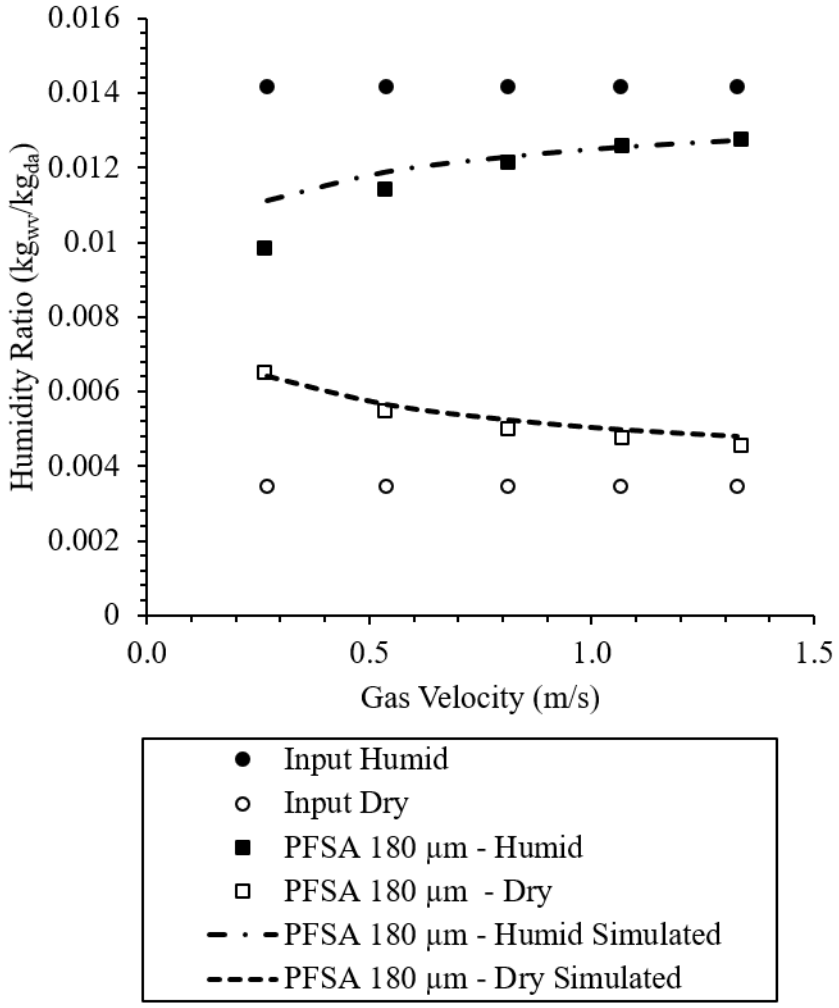

Figure 37: A comparison of the measured outlet humidity ratio of a 3.1 mm channel depth with a 180 µm PFSA membrane to the simulated results from down the channel model from a sweep gas experiment.

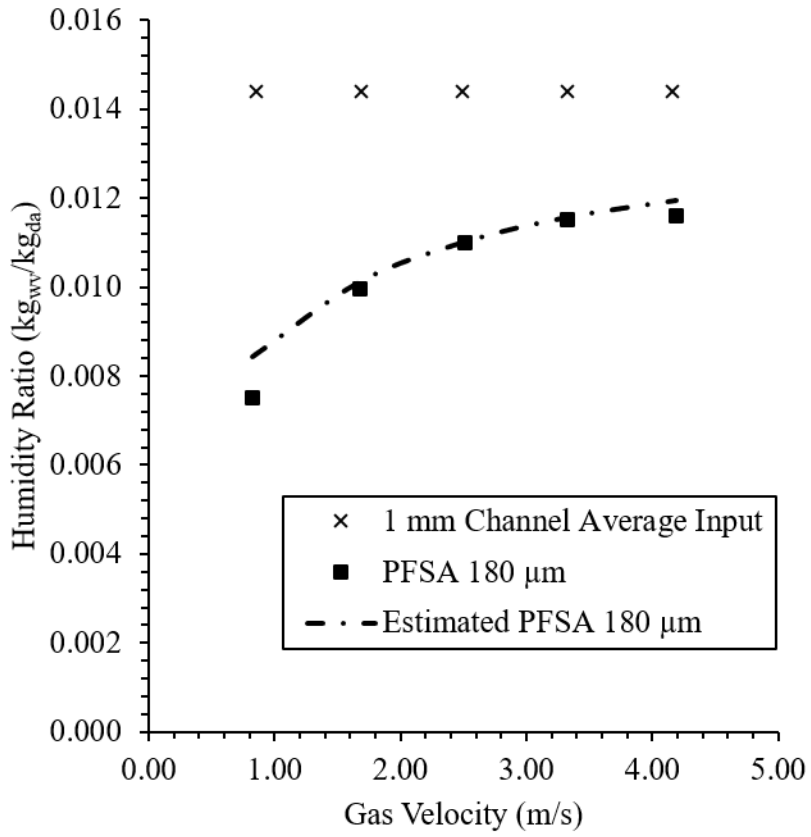

Figure 38: A comparison of the measured outlet humidity ratio of a 1 mm channel depth with a 180 µm PFSA membrane to the simulated results from the down the channel model for a vacuum pressure experiment.

The down the channel model was then applied to report humidity ratios as a function of channel length as a method to determine the useful length of a channel for varying flow rate, channel depth and membrane thickness. Figure 39 displays the simulated humidity ratio throughout the length of a 0.5 mm channel at 1.7, 5.0, and 8.3 m/s. As the gas moves through the channel, the concentration gradient decreases and as a result the rate of water vapor transfer decreases. Additionally, due to the small channel depth, the convection resistance is nearly equal to the diffusion resistance.

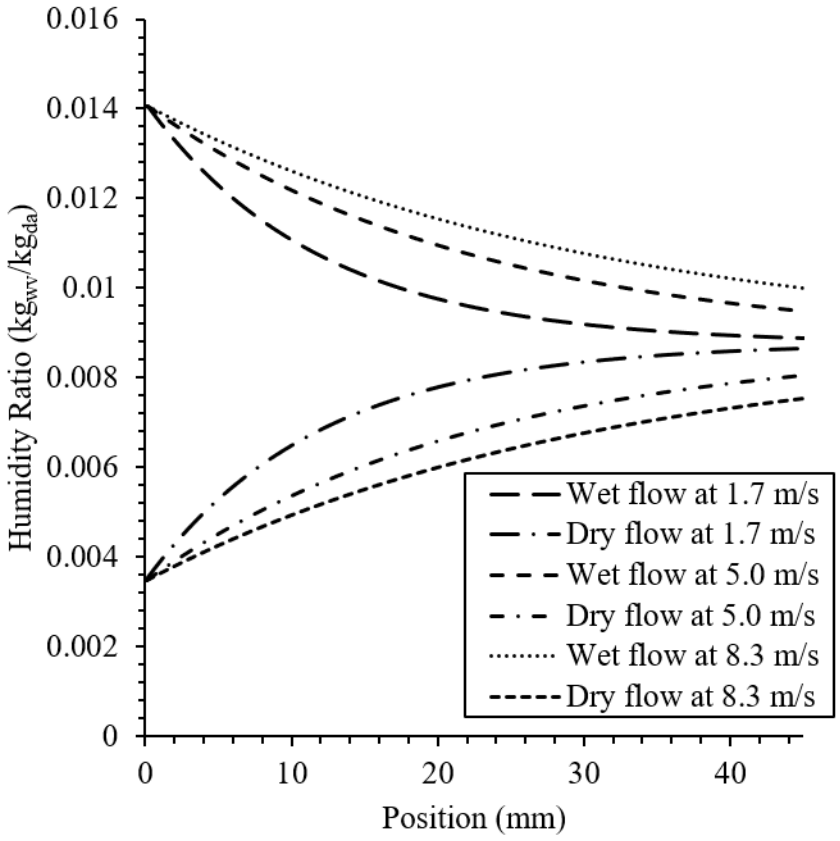

Figure 39: A simulation of the humidity ratio through the length of the channel with a 25 µm PFSA membrane in a 0.51 mm channel at three different gas velocity (Sweep Gas Experiments)

In deeper channels convective resistance is much greater than the diffusion resistance through the membrane. As a result, the change in humidity ratio is nearly linear. This can be seen in Figure 40 throughout the length of the channel.

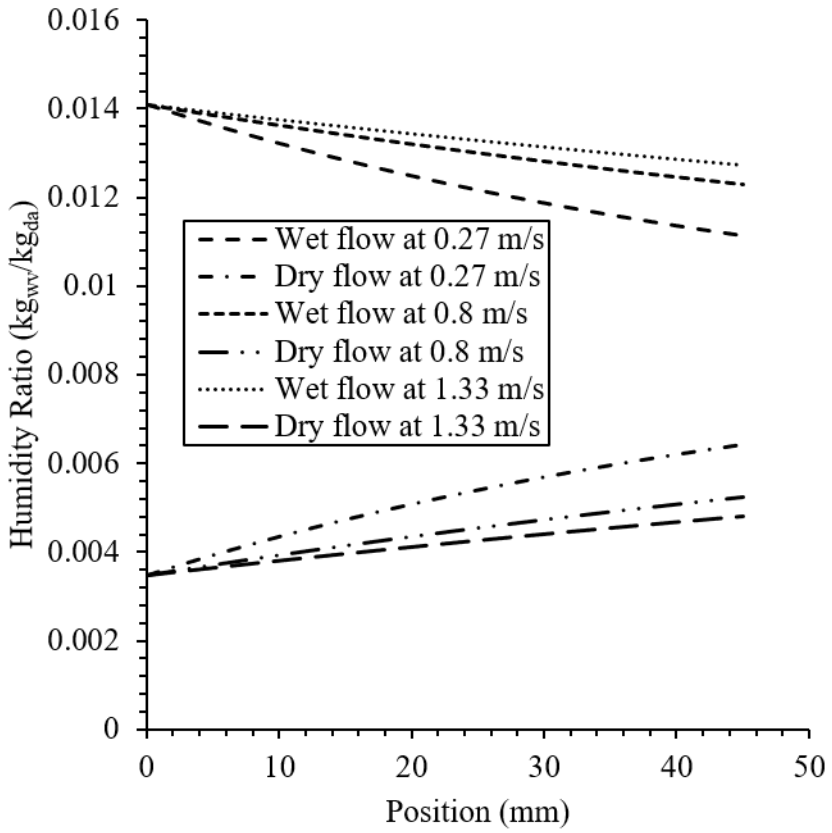

Figure 40: A simulation of humidity ratio throughout the channel length in a 3.13 mm channel at three different gas velocities with a 180 µm membrane. (Sweep Gas Experiments)

4.3 The Modeling and Performance of an MHP Dedicated Outdoor Air System (DOAS)

A DOAS is responsible for managing the latent and sensible cooling for incoming ventilation air. These systems are comprised of many subsystems such as vapor compression heat pumps, desiccant wheels, energy recovery cores, and a pair of mass exchangers. This section provides an overview of each subsystem and the assumptions made for each subsystem required for the modeling of an MHP DOAS system.

4.3.1 System Schematic

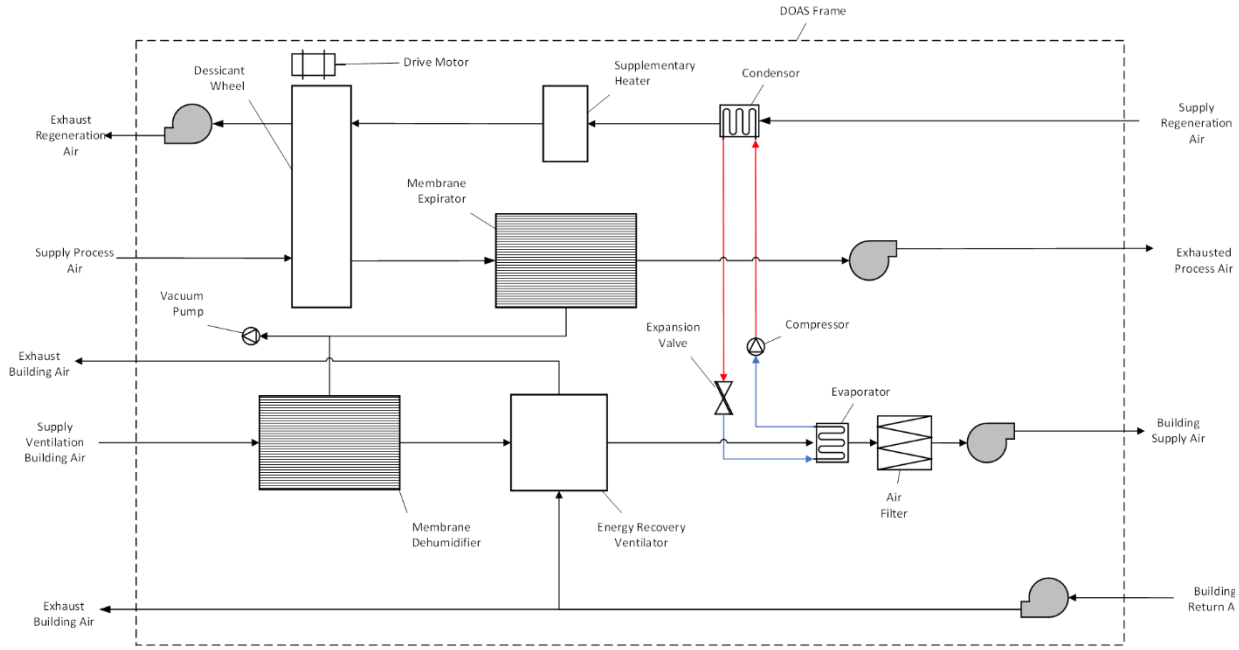

Figure 41: An MHP DOAS system diagram

The DOAS as seen in Figure 41, manages four different air flows. The first air flow is used to regenerate the desiccant wheel. This air flow is heated by the condenser of a vapor compression system and a supplementary heater. After passing through the desiccant wheel, the air is exhausted out of the unit. A second air flow is passed through the desiccant wheel and is dehumidified to at minimum a humidity ratio of 0.0086 $kg_{water\ vapor}/kg_{dry\ air}$. The air then passes through the expirator mass exchanger where it is humidified and then exhaust outdoors. The building supply air enters

the DOAS and is dehumidified by a mass exchanger to the building setpoint. The air then passes through an energy recovery ventilator where it is partially cooled, followed by a vapor compression system to complete the rest of the necessary sensible cooling. The final air flow is the building exhaust air, which is either pushed directly outdoors or is used to manage the initial sensible cooling of the building supply air.

The vacuum pump is responsible for roughing the system to 1.25kPa, after which it is shut off. The expirator removes water vapor from the vacuum plenum at the same rate that water vapor is removed from the supply building air stream. After start up, the vacuum pump is required to intermittently return the system to 1.25kPa as a result of the diffusion of oxygen, nitrogen, etc. For this analysis, the electrical load required for system roughing and intermittent maintenance of system pressure from a vacuum pump is assumed to be negligible due to the high selectivity of water vapor from the PFSA membrane. Additionally, it was assumed that all building exhaust air was directed to the energy recovery ventilator.

The supplemental heat for this simulation was not included when determining the realized COP. Thermal integration of buildings has become common method of saving energy by using waste heat streams as a power source for other building activities. As a result, it was assumed that any required supplemental heat was provided at no energy cost to the system. This energy could come from a cooling loop from manufacturing equipment, combined heat and power system (CHP), or other processes exhausting a low-grade waste heat stream.

4.3.2 Model Set-up

The DOAS simulation was developed to best represent the working conditions of a 3-rTon of latent cooling for air at 80% RH with a dry bulb temperature of 23 °C while at 1 atm with a building setpoint of 50% RH. From this, the system flow rate was determined to be approximately

2650 m^3/hr (1550 cfm). Each subcomponent was sized individually, and energy input requirements were based on reported or calculated COP's of commercially available components as functions of the water removal rate or the input dry bulb temperature.

4.3.3 Desiccant Wheel

A software developed by Rotor Source, Inc [32] was used to estimate a COP based on the latent cooling completed for 2646 m^3/h (1557 cfm) of air at 23 °C dry bulb and 80% RH. A screenshot of the software can be seen in Figure 42.

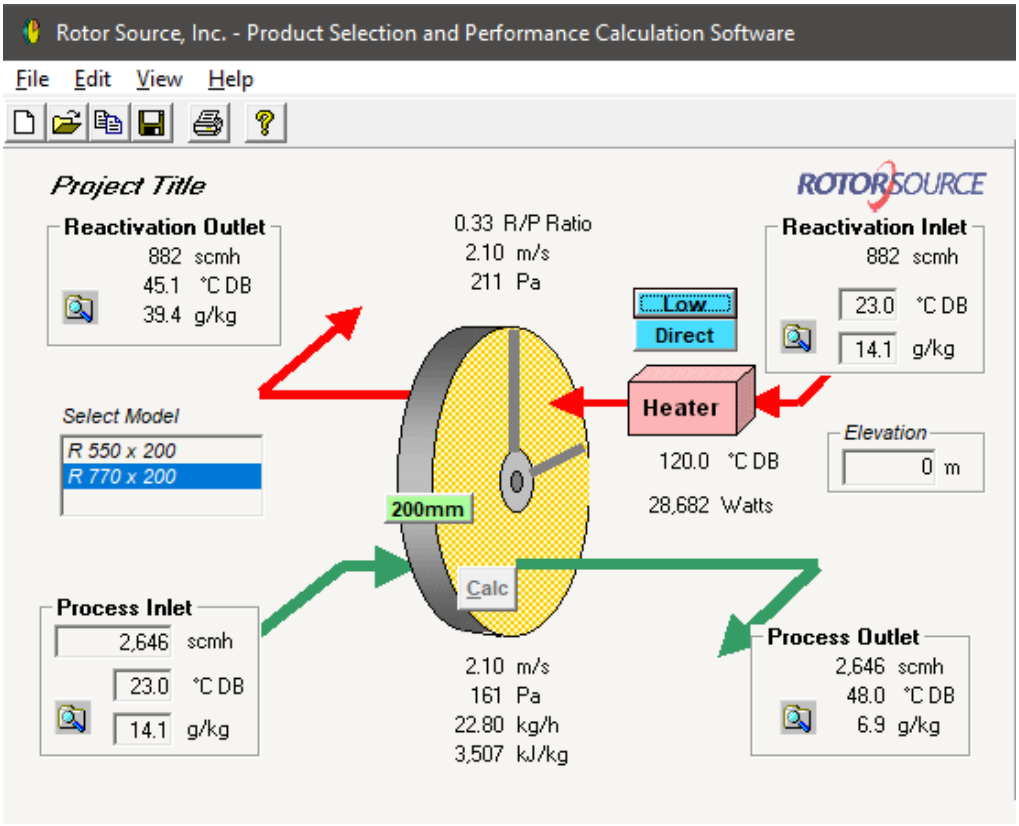

Figure 42: Rotor Source, Inc Software used to determine the COP of a desiccant wheel for a 3-rTon DOAS system [32]

The energy requirements of the desiccant wheel are determined from the power required to overcome the pressure drop of the desiccant wheel, the input required heat, and the motor used to rotate the wheel. Table 5 contains all sizing parameters for the selected desiccant wheel along

with the calculated COP. The COP of the desiccant wheel was determined using the following equation:

$$COP = \frac{Latent\ Cooling}{Total\ Power\ Input} \qquad \textit{Equation 8}$$

Table 5: Selected parameters of the desiccant wheel

Parameter	Value
Dry Bulb Temperature	23.0 °C
Process Air Flow Rate	2646 m^3/hr
Regeneration Air Flow Rate	882 m^3/hr
Process Air Input Humidity Ratio	14.1 $g_{water\ vapor}/kg_{dry\ air}$
Process Air Output Humidity Ratio	6.9 $g_{water\ vapor}/kg_{dry\ air}$
Heater Temperature	120 °C DB
Process Air Pressure Drop	161 Pa
Regeneration Air Pressure Drop (Excluding heater)	211 Pa
Process Air Blower Efficiency	55%
Regeneration Air Blower Efficiency	55%
Process Air Blower Power	0.2 kW
Regeneration Air Blower Power	0.1 kW
Heat Required	28.7 kW
Rotor Motor Power	0.04 kW
Total Thermal Energy Input	28.7 kW
Total Mechanical Energy Input	0.3 kW
Latent Cooling Achieved	19.8 kW
COP	0.68

4.3.4 Vapor Compression System.

The vapor compression system was sized to account for the total sensible load. However, the simulation of the vapor compression system worked in conjunction with the energy recovery ventilator. The energy recovery ventilator was modeled after a commercially available system with a 65% sensible energy recover [33]. The remaining sensible cooling was completed by a vapor compression system.

The selected vapor compression system for the simulation was rated for 5 Ton of sensible cooling at a COP of 4.4 (SEER 15) [34]. The electrical energy consumption was determined by:

$$Power\ Required = \frac{\dot{m}_{air} c_p [(\Delta T)(1 - \eta_{ERV})]}{COP} \qquad \textit{Equation 9}$$

where $\dot{m}_{air}$ is the mass flow rate of air, c_p is the specific heat of air, ΔT is the change in temperature and η_{ERV} is the efficiency of the energy recover ventilator from 0-1.

4.3.5 Mass Exchanger (ME) Design

For the simulation, the dehumidification mass exchanger was assumed to have the same mass transfer properties per square meter of membrane as the expiration system. All geometry considerations for the dehumidification mass exchanger are the same for the expirator. A PFSA membrane with a thickness of 50 µm and a diffusion coefficient of 0.07 cm^2/s. To make this assumption, the humidity ratio supplied to the expirator must be adequately below the outlet humidity ratio of the dehumidification mass exchanger. To ensure this, the selected desiccant wheel was oversized by 15%.

To determine the aspect ratio of the mass exchanger, a study on the required length for three different channel depths was completed. The selected channel depths were 0.5 mm, 1.0 mm and 2.0 mm. The input relative humidity was 80% at 23 °C. The required outlet humidity was 50% at 23 °C. The mass exchanger width was 0.3 m. The length of the mass exchanger was then determined along with the pressure drop. The pressure drop and volumetric flow rate were used to determine the pumping losses for each gap width. The latent cooling and pumping losses were normalized over the active area of the membrane and is displayed by Figure 43.

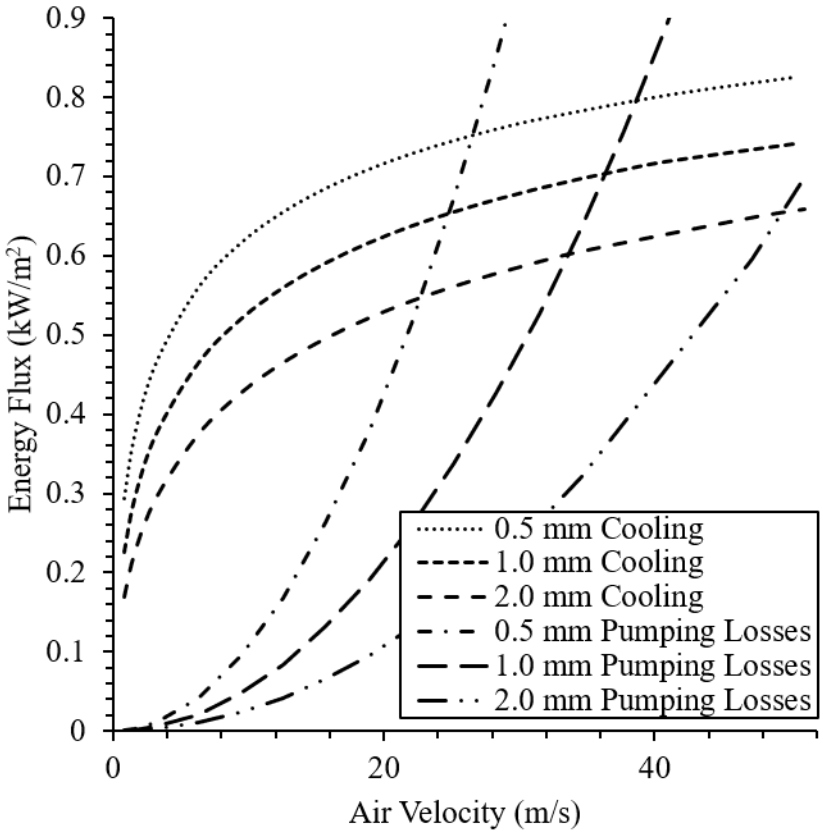

Figure 43: Cooling Achieved and Pumping Losses per square meter of membrane for 3 different channel depths

As velocity increases, the rate of latent cooling increases in a logarithmic manor. The small channel yielded the greatest cooling potential per meter squared of membrane as expected since the convective resistance in the channel is the lowest. The pressure drops of the 0.5 mm channel increased at the quickest rate. To get a better understanding of the tradeoff between latent cooling density and velocity in the channel, the effective latent cooling was determined from:

$$Effective\ Latent\ Cooling\ = \frac{Latent\ Cooling - Pumping\ Losses}{Membrane\ Active\ Area} \qquad \textit{Equation 10}$$

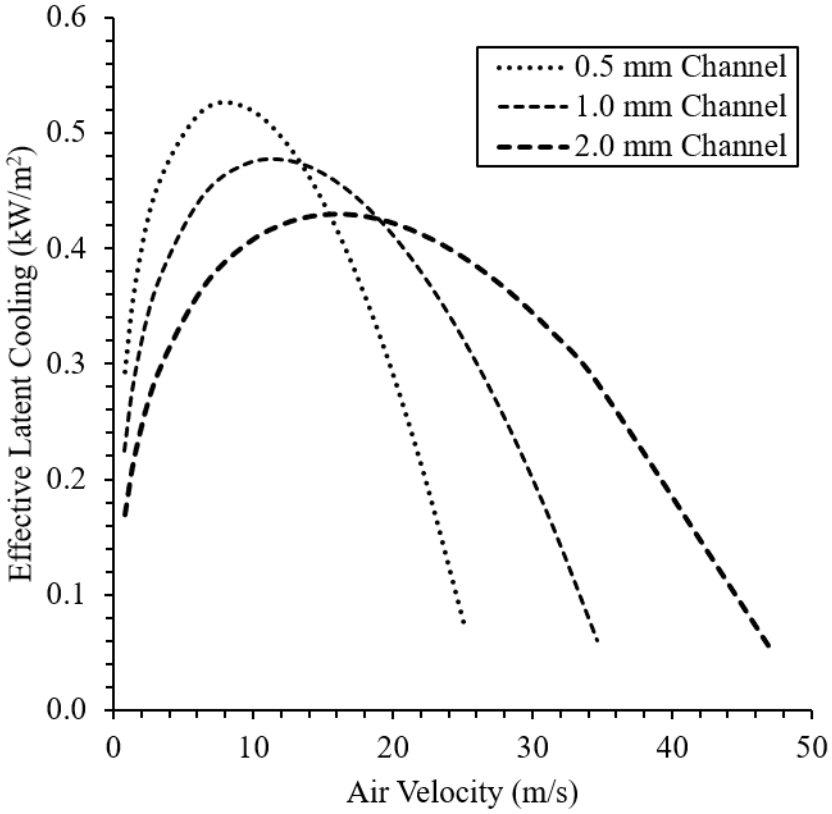

Figure 44: Effective Cooling per square meter of membrane

The results from Figure 44 display the tradeoff between energy loss as a result of pressure drop through the mass exchanger and the amount of latent cooling achieved per square meter of membrane area. As a result, five mass exchangers were considered for the simulation. The first three design parameters match to the greatest effective cooling achieved for each gap width. These design parameters are seen in Table 6, Table 7, and Table 8. The remaining two mass exchanger configurations were selected to meet ASHRAE standard 62 for pressure drop and velocity. These configurations are seen in Table 9 and Table 10.

Table 6: Mass Exchanger #1 (ME #1)

Parameter	Value
Gap Width	0.5 mm
Exchanger Width	0.30 m
Exchanger Length	0.1 m
Active Area/Plate	0.03 m^2
Membrane Area	17.1 m^2
Air Velocity	9.44 m/s
Latent Cooling / sq. meter	0.62 kW/m^2
Pressure Drop	610 Pa

Table 7: Mass Exchanger #2 (ME #2)

Parameter	Value
Gap Width	1.0 mm
Exchanger Width	0.3 m
Exchanger Length	0.32 m
Active Area/Plate	0.09 m^2
Membrane Area	18.8 m^2
Air Velocity	12.6 m/s
Latent Cooling / sq. meter	0.56 kW/m^2
Pressure Drop	599 Pa

Table 8: Mass Exchanger #3 (ME #3)

Parameter	Value
Gap Width	2.0 mm
Exchanger Width	0.3 m
Exchanger Length	0.9 m
Active Area/Plate	0.27 m^2
Membrane Area	21.3 m^2
Air Velocity	15.73 m/s
Latent Cooling / sq. meter	0.5 kW/m^2
Pressure Drop	532 Pa

Table 9: Mass Exchanger #4 (ME #4)

Parameter	Value
Gap Width	1.0 mm
Exchanger Width	0.3m
Exchanger Length	0.1 m
Active Area/Plate	0.03 m^2
Membrane Area	30.7 m^2
Air Velocity	2.44 m/s
Latent Cooling / sq. meter	0.34 kW/m^2
Pressure Drop	36.7 Pa

Table 10: Mass Exchanger #5 (ME #5)

Parameter	Value
Gap Width	2.0 mm
Exchanger Width	0.3 m
Exchanger Length	0.26 m
Active Area/Plate	0.08 m^2
Membrane Area	39.5 m^2
Air Velocity	2.44 m/s
Latent Cooling / sq. meter	0.27 kW/m^2
Pressure Drop	23.7 Pa

4.3.6 Centrifugal Blower Sizing

The system used centrifugal blowers or regenerative blowers with an efficiency of 70% or 55%, respectively. The power required to move air throughout the system was determined by Equation 11.

$$Power_{blower} = \frac{\Delta P \dot{V}}{\eta_{blower}} \qquad \textit{Equation 11}$$

In Equation 11, η_{blower} is the blower efficiency, ΔP is the pressure drop in the air stream, and $\dot{V}$ is the volumetric flow rate.

4.3.7 MHP DOAS System Performance

The previous sections outline the individual parameters taken into consideration for modeling the efficiency of each component. This section will discuss how each system was incorporated into the MHP DOAS simulation.

The desiccant wheel was assumed to have a consistent ratio of heat required to latent cooling achieved of 1.45:1. To determine the heater energy requirement the thermal energy for each operating condition was calculated by Equation 12.

$$Thermal\ Energy\ Required = \frac{Latent\ Cooling\ from\ Mass\ Exchanger}{0.69} \qquad \textit{Equation 12}$$

The pressure drop through the desiccant wheel was considered constant as flow rate for each point was not varied. Additionally, the energy required to rotate the wheel was considered constant. The supplemental heater was assumed to have a pressure drop of 75 Pa.

The required sensible cooling was determined based on the dry bulb temperature for each condition at the outlet of the energy recovery ventilator. The energy recovery ventilator only completed sensible cooling. The pressure drop through the energy recover ventilator was assumed to be 100 Pa. The pumping losses in the HVAC duct were considered negligible when compared to the pressure drop in each system component and were therefore not included in the analysis.

Depending on the mass exchanger configuration, the efficiency of the blower was varied. For ME #1, #2 and #3, the blower efficiency was assumed 55% as there was a greater amount of pressure drop to overcome and would require the use of a regenerative blower. For the configurations that used ME #4 and #5, a blower efficiency of 70% was selected to represent a centrifugal blower. The blower efficiency of 80% was assumed for the building return air. Each simulation was completed with consistent assumptions for each system configuration.

In the first simulation, the model was given an increasing dry bulb temperature while the RH at each dry bulb temperature was maintained at 80%. As seen in Figure 45, as the dry bulb temperature increased, the change in wet bulb temperature at the outlet of the ME increased. The increased change in wet bulb temperature from inlet to outlet is a result of an increasing concentration differential of water vapor in the supply air stream to the vacuum side of the mass exchanger. The outlet wet bulb temperature for each ME was similar and as a result only the simulation data for ME# 1 is displayed.

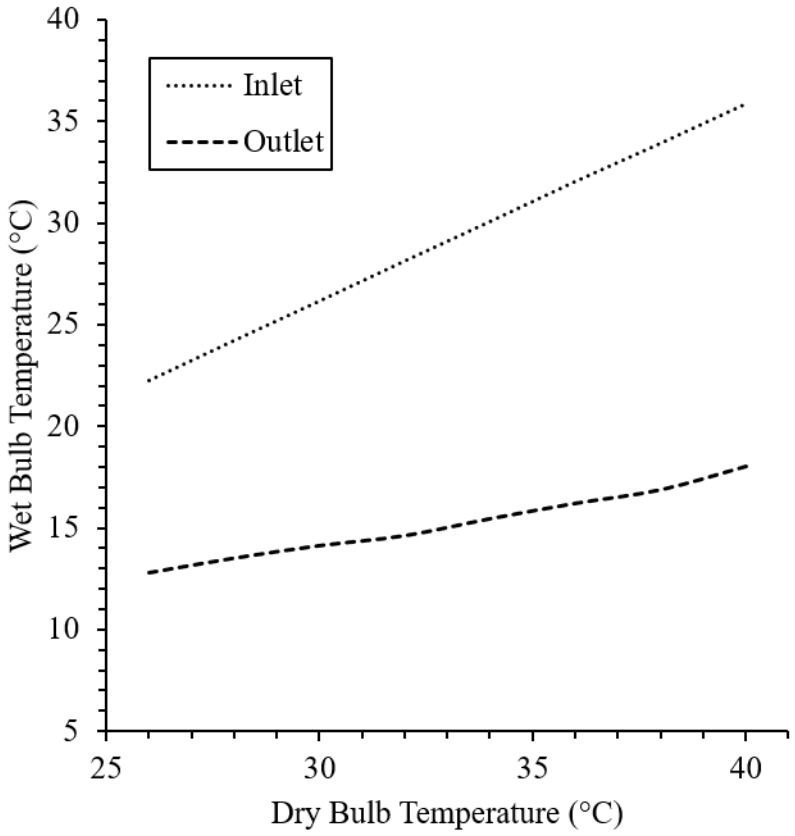

Figure 45: A comparison of the inlet dewpoint and outlet dewpoint as dry bulb temperature was increased for an MHP DOAS configured with ME# 1

The COP for each MHP DOAS was determined for the system as an overall COP and a electrical COP. The overall COP considers all input energy, thermal and electrical. The electrical

COP assumes the building has been thermally integrated to the MHP DOAS system such that the thermal energy required is sourced from an existing waste heat stream. The electrical COP is determined using the following formula:

$$COP_{electrical} = \frac{Latent\ Cooling}{Electrical\ Power\ Input} \qquad \textit{Equation 13}$$

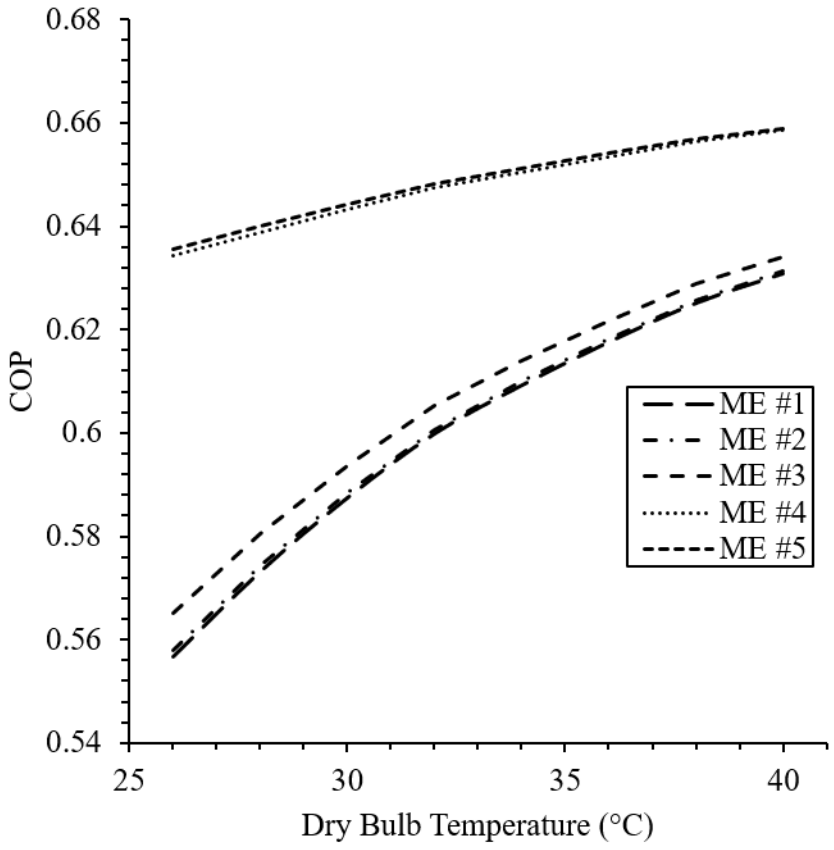

Figure 46: COP for the various configurations of ME in an MHP DOAS

Figure 46 and Figure 47 display the total COP and electrical COP of the various MHP DOAS configurations. In both figures, the COP increases as the input dry bulb temperature increases. ME #1, 2 and 3 did not perform as well as ME #3 and ME #4. This is a result of the greater amount of pressure drop in the ME and the less efficient pump required to overcome the pressure drop.

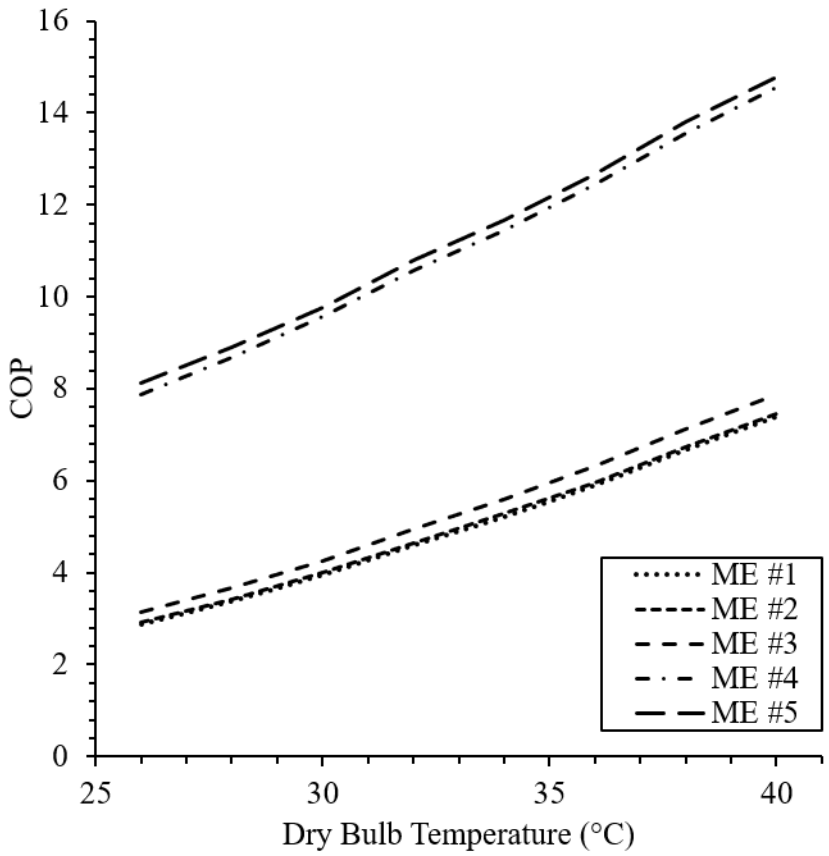

Figure 47: Electrical COP for different configurations of an MHP DOAS Configuration

If the thermal energy requirements of the MHP DOAS system are no longer considered an energy penalty to the system efficiency, i.e. thermally integrated to a building waste heat source, and the electrical energy input is considered the only energy input, the COP improves for each ME configurations.

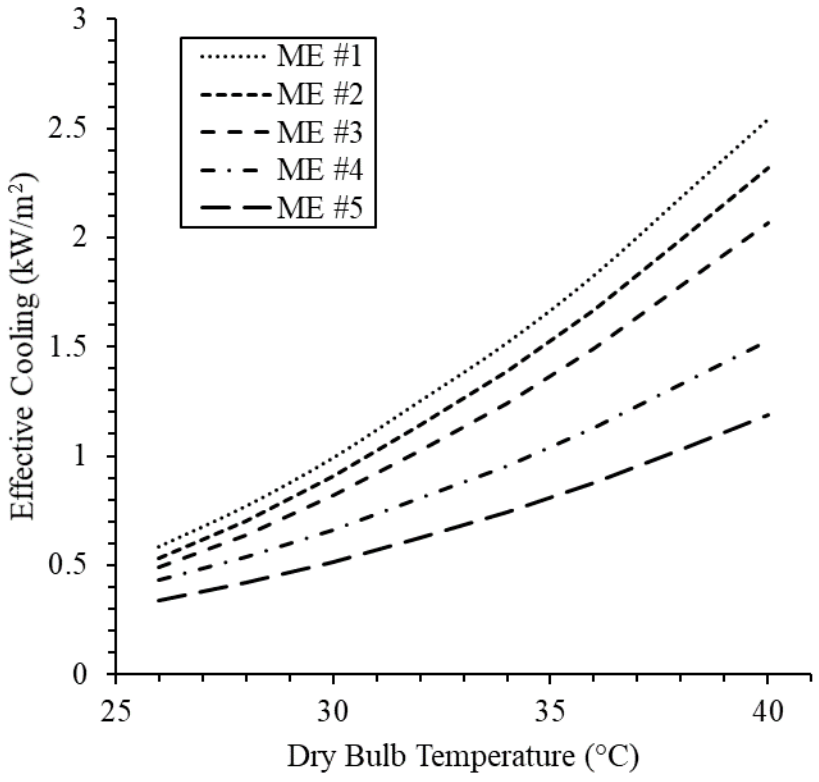

Figure 48: Effective cooling per square meter for five different MHP DOAS configurations

For each MHP DOAS configuration, the effective cooling per square meter was determined. Figure 46, Figure 47, Figure 48 and Figure 49 when viewed together display the tradeoff of between membrane required, initial cost and performance. As seen in Figure 48, ME #1, #2, and #3 display the greatest effective cooling flux, respectively, followed by ME #4 and #5. The designs of ME #1, ME #2 and ME #3 yield high flow rate within the channel to reduce convective resistance and to reduce the amount of membrane required. In summary, these MEs are diffusion limited or diffusion controlled. In ME #4 and ME #5, the convective resistance is greater than the diffusion resistance thus requiring more membrane in the system.

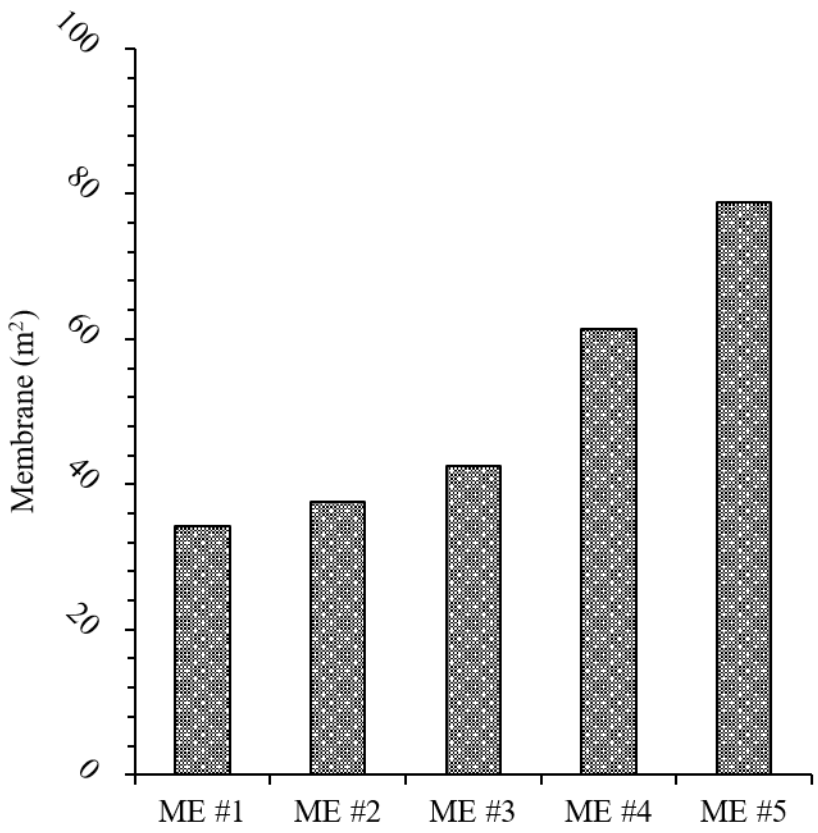

Figure 49: A comparison of the required membrane area for each ME configuration

The MHP concept reviewed shows promise that an electrical COP greater than 7.5 can be achieved for the sensible and latent cooling required in DOAS system. Current vapor compression systems operate with a COP between 3.5 and 4.5 [35,36]. Desiccant wheels typically operate with a COP between 0.5 – 0.6 and require a substantial amount of sensible cooling to return the air to the proper supply air temperature [37].

5. Conclusion

Latent cooling without phase change could potentially reduce the energy required for air conditioning. Water selective membranes are a key enabler for many technologies aimed at achieving this goal. Numerous membrane materials have been developed and characterized for water selectivity and transport performance with high process gas flow. The current study was developed to consider a subset of these materials along with practical design requirements of commercial HVAC systems that constrain process air flow and pressure loss. These parameters ultimately translate to high convective mass transport resistance of water vapor through air in the mass exchanger. Experiments varying membrane thickness and gas flow gap were used to separately measure membrane and channel transport resistance. The collected datas were used to validate an empirical down the channel mass transfer model. The validated mass transfer model was then applied to simulate a 3 rTon MHP DOAS system for various mass exchanger geometries under consistent conditions. From the resulting studies, multiple findings were concluded and can be summarized by the following:

1. Using the two experiments, convection resistance in channels ranging from 0.5 mm to 3.1 mm was measured and diffusion resistance through the PFSA membrane was characterized at four different membrane thicknesses.
2. Convection resistance is up 6x's greater than diffusion resistance for typical HVAC conditions for pressure drop and gas velocity.
3. The observed convective resistances of the 4 channel depths were used to validate Sherwood number correlations that can be used to empirically model mass transfer.

4. The in-channel flow characteristics required to reach the greatest effective latent cooling per square meter of membrane surpasses the ASHRAE standards for pressure drop and air velocity.
5. A comparison of five different mass exchangers geometries encompassed within a MHP DOAS was completed with results that show the tradeoff of effective latent cooling per square meter of membrane, system COP and required membrane active area.
6. The MHP DOAS simulation results show that a total COP of 0.5 to 0.7 was achieved when considering both the required thermal and electrical energy inputs to the system.
7. The COP of the MHP DOAS system based on the electrical input only is greater than 7.5 for mass exchangers designed to meet ASHRAE standards with 1.0 mm and 2.0 mm channel depths.
8. An MHP DOAS that is designed to meet ASHRAE standards is capable of achieving a COP that is 50% higher than comparable vapor compression DOAS.
9. Mass exchangers designed my maximum effective latent cooling result in significant pumping losses which reduce the electrical COP to less than 4 for the simulated conditions.

6. Future Considerations

Future considerations should focus on maximizing convection within the channel while meeting the design criteria set by ASHRAE. Employing obstacles in designs for channels greater than 1.0 mm in channel depth show promise that the rate of mass transfer can be further improved. Additional modeling that considers the system location, the location's average weather data, and the use of variable speed pumps would identify regions and climates that the system will perform the best. Lastly, durability is great importance for HVAC systems. Studies that outline the expected working hours of various membrane materials for conditions that relate to a membrane based HVAC system and that list the key environmental conditions that affect the working life will provide valuable insight for a life-cycle cost analysis and maintenance requirements if adopted within the HVAC market.

References

[1] U.S. Energy Information Administration, Annual Energy Outlook 2017 with projections to 2050, 2017. https://doi.org/DOE/EIA-0383(2017).

[2] L.G. Harriman, D. Plager, D. Kosar, Dehumidification and cooling loads from ventilation air, Energy Eng. J. Assoc. Energy Eng. (1997). https://doi.org/10.1080/01998595.1999.10530479.

[3] California Air Resources Board, High-GWP Refridgerants, (2007).

[4] P.W. Gibson, Effect of temperature on water vapor transport through polymer membrane laminates, Polym. Test. 19 (2000) 673–691. https://doi.org/10.1016/S0142-9418(99)00040-9.

[5] R. Xing, Y. Rao, W. TeGrotenhuis, N. Canfield, F. Zheng, D.W. Winiarski, W. Liu, Advanced thin zeolite/metal flat sheet membrane for energy efficient air dehumidification and conditioning, Chem. Eng. Sci. (2013). https://doi.org/10.1016/j.ces.2013.08.061.

[6] S.J. Metz, W.J.C. Van De Ven, J. Potreck, M.H.V. Mulder, M. Wessling, Transport of water vapor and inert gas mixtures through highly selective and highly permeable polymer membranes, J. Memb. Sci. (2005). https://doi.org/10.1016/j.memsci.2004.08.036.

[7] Z. Ogumi, Gas Permeation in SPE Method, J. Electrochem. Soc. (2006). https://doi.org/10.1149/1.2115696.

[8] R.W. Gore, S.B.J. Allen, Waterproof laminate, US05920275, 1978.

[9] J. Woods, Membrane processes for heating, ventilation, and air conditioning, Renew. Sustain. Energy Rev. (2014). https://doi.org/10.1016/j.rser.2014.01.092.

[10] O. Labban, T. Chen, A.F. Ghoniem, J.H. Lienhard, L.K. Norford, Next-generation HVAC: Prospects for and limitations of desiccant and membrane-based dehumidification and

cooling, Appl. Energy. (2017). https://doi.org/10.1016/j.apenergy.2017.05.051.

[11] P. Scovazzo, A.J. Scovazzo, Isothermal dehumidification or gas drying using vacuum sweep dehumidification, Appl. Therm. Eng. (2013). https://doi.org/10.1016/j.applthermaleng.2012.05.019.

[12] H.T. El-Dessouky, H.M. Ettouney, W. Bouhamra, A novel air conditioning system: Membrane air drying and evaporative cooling, Chem. Eng. Res. Des. (2000). https://doi.org/10.1205/026387600528111.

[13] J. Owejan, N. DeMario, Latent and sensible cooling membrane heat pump, US10502438B2, n.d.

[14] EERE, Energy Savings Potential and RD&D Opportunities for Non-Vapor-Compression HVAC Technologies, Washington DC, 2014. https://doi.org/10.2172/1220817.

[15] R.S. Das, S. Jain, Experimental performance of indirect air-liquid membrane contactors for liquid desiccant cooling systems, Energy. (2013). https://doi.org/10.1016/j.energy.2013.05.013.

[16] ANSI, ANSI/ASHRAE Standard 62.1-2010, Ventilation for Acceptable Indoor Air Quality, ASHRAE. (2007). https://doi.org/ANSI/ASHRAE Standard 62.1-2004.

[17] ASHRAE, ASHRAE hand book HVAC system and equipment, 2016. https://doi.org/10.1017/CBO9781107415324.004.

[18] A.A. Bukshaisha, B.M. Fronk, Simulation of membrane heat pump system performance for space cooling, Int. J. Refrig. (2019). https://doi.org/10.1016/j.ijrefrig.2018.12.010.

[19] EERE, Energy Savings Potential and RD&D Opportunities for Commercial Building HVAC Systems, Washington DC, 2017.

[20] K.J. Chua, S.K. Chou, W.M. Yang, J. Yan, Achieving better energy-efficient air

conditioning - A review of technologies and strategies, Appl. Energy. (2013). https://doi.org/10.1016/j.apenergy.2012.10.037.

[21] Comparative performance study of vapour compression refrigeration system with R22/R134a/R410A/R407C/M20, Int. J. Energy Environ. (2011).

[22] Dias Analytic Inc, Dias, NanoAir, (n.d.). https://daisanalytic.com/applications/nanoair/.

[23] B. Yang, W. Yuan, F. Gao, B. Guo, A review of membrane-based air dehumidification, Indoor Built Environ. (2015). https://doi.org/10.1177/1420326X13500294.

[24] R. Ray, D.D. Newbold, S.B. McCray, D.T. Friesen, M. Kliss, A novel membrane device for the removal of water vapor and water droplets from air, in: SAE Tech. Pap., 1992. https://doi.org/10.4271/921322.

[25] M. Adachi, Proton Exchange Membrane Fuel Cells : Water Permeation Through Nafion Membranes, 2010.

[26] P. Majsztrik, A. Bocarsly, J. Benziger, Water permeation through nafion membranes: the role of water activity, J. Phys. Chem. B. 112 (2008) 16280–16289. https://doi.org/10.1021/jp804197x.

[27] B. Smitha, S. Sridhar, A.A. Khan, Solid polymer electrolyte membranes for fuel cell applications - A review, J. Memb. Sci. (2005). https://doi.org/10.1016/j.memsci.2005.01.035.

[28] T.A. Zawodzinski, Water Uptake by and Transport Through Nafion® 117 Membranes, J. Electrochem. Soc. 140 (1993) 1041. https://doi.org/10.1149/1.2056194.

[29] M. Drinkmann, Structure and Processing of SYMPATEX Laminates, J. Ind. Text. 21 (1992) 199–211. https://doi.org/10.1177/152808379202100306.

[30] M. Adachi, Proton Exchange Membrane Fuel Cells : Water Permeation Through Nafion

Membranes, Simon Fraser Univ. (2010).

[31] Y.A.C.& A.J. Ghajar, Heat and Mass Transfer: Fundamentals & Applications, 1986. https://doi.org/10.1017/CBO9780511676420.004.

[32] I. Rotor Source, Product Selection and Performance Calculation Software, (n.d.). https://www.rotorsource.com/desiccant-dehumidification.

[33] AnnexAir, Heat recovery ventilator with a fixed plate, (n.d.). https://www.annexair.com/Portals/0/Our Products/PDF/ERU-FPlate_erv.pdf.

[34] Daikin, DTH Commercial 3 - 5 Ton Heat Pumps, (2018). https://www.daikinac.com/content/assets/LightCommercial/PackagedSystems/DTH Series 3-5 tons/SS-DTH3.pdf (accessed January 3, 2020).

[35] Goodman, GPC14H, (2018).

[36] Ingersoll Rand, Trane True Comfort Variable Speed Systems, (2015).

[37] M.G. Rasul, A.K. Azad, S.C. Sharma, Clean energy for sustainable development: Comparisons and contrasts of new approaches, 2016.